Eur. J. Mineral., 34, 301–319, 2022
https://doi.org/10.5194/ejm-34-301-2022
© Author(s) 2022. This work is distributed under
the Creative Commons Attribution 4.0 License.

European Journal of Mineralogy
Open Access

Firing and post-firing dynamics of Mg- and Ca-rich bricks used in the built heritage of the city of Padua (northeastern Italy)

Elena Mercedes Pérez-Monserrat[1], Lara Maritan[1], and Giuseppe Cultrone[2]

[1]Department of Geosciences, University of Padua, Padua, 35131, Italy
[2]Department of Mineralogy and Petrology, Faculty of Sciences, University of Granada, Granada, 18071, Spain

Correspondence: Elena Mercedes Pérez-Monserrat (elenamercedes.perezmonserrat@unipd.it)

Received: 10 January 2022 – Revised: 8 April 2022 – Accepted: 19 April 2022 – Published: 19 May 2022

Abstract. Diverse types of bricks from monuments in the city of Padua (northeastern Italy) were studied using a multi-analytical approach based on spectrophotometry, X-ray fluorescence (XRF), X-ray powder diffraction (XRPD), polarized-light optical microscopy (POM) and/or high-resolution scanning electron microscopy with coupled energy-dispersive X-ray spectroscopy (HRSEM-EDS). The most representative bricks were yellow or beige and in well-preserved condition. The results showed that they were made of Mg- and Ca-rich illitic clays, were fired at high temperatures (from 900 to over 950 °C), and achieved an incipient vitrification. Two main processes took place during firing: (i) the development of a Ca-aluminosilicate amorphous phase where very abundant pyroxene-type crystals were nucleated and (ii) the transformation of the pristine Mg-rich clayey grains into Mg-silicate mineral phases. The analyses suggest a firing dynamic within a highly reactive and supersaturated unstable system, particularly rich in calcium and magnesium. There are also signs of the rapid heating and/or soaking of the bricks and the irregular heat distribution and/or different residence times inside the kilns. The formation of zeolite and calcite secondary phases was also observed. The former was largely promoted by the high calcium content of the bodies and the very humid conditions, while the latter was mainly precipitated from Ca-rich solutions. The preservation of the bricks was enhanced by processes that took place both during and after firing. Firstly, the significant development of a Ca-rich amorphous phase and of high-temperature pyroxene-type crystals has provided strength to the bricks. Secondly, the porosity yielded by the firing of the carbonate-rich clays was almost filled by secondary calcite, which acted as a cementing agent. The information attained has increased the knowledge of (i) the mineralogical and microstructural changes that take place during the firing over 900 °C of Ca- and Mg-rich illitic clays and (ii) the formation of secondary phases within highly calcareous bricks laid in very humid environments and affected by Ca-rich solutions. The key role of the Ca- and Mg-rich raw clays and of the high firing temperatures, in producing high-quality bricks, and of the secondary calcite, which increased their durability, is highlighted. All these factors have contributed to the better preservation of the built heritage of the city.

1 Introduction

The firing of raw clays entails a dynamic and disequilibrium system in which two main stages take place: the decomposition of the original minerals of the raw clays and the formation of new phases (Shoval, 1988; Riccardi et al., 1999). The dehydroxylation of clay minerals contributes to the development of an amorphous silicate phase that diminishes with increasing temperature, as the newly formed phases nucleate and grow (Rathossi and Pontikes, 2010; Heimann and Maggetti, 2019). The firing of carbonate-rich clays gives rise to newly formed silicates from around 800 °C (Peters and Iberg, 1978) that enhance the compressive strength of the resulting ceramic products (Celik et al., 2019). The fluid phase generated by carbonate decomposition improves reaction kinetics, diffusion and nucleation processes, which are mostly

controlled by the water and carbon dioxide released at different temperatures as a result of dehydration and decarbonation processes (Duminuco et al., 1998).

Clays with abundant carbonates tolerate a wide range of firing temperatures and result in ceramics with exceptional porosity, mechanical behavior and weather resistance (Kingery and Aronson, 1990; Tite, 1991). The reaction of carbonates and silicates at high temperatures yields newly formed phases such as melilites and pyroxenes (Peters and Iberg, 1978; Trindade et al., 2009; Cultrone and Carrillo, 2020). Despite the fact that Mg-rich clays may yield highly resistant ceramics at low firing temperatures (Lagzdina et al., 1998; Darweesh, 2001), much more research has been carried out on the decomposition and reaction products of calcite than on those of dolomite (Gliozzo, 2020).

In research on historic ceramics, in addition to the residual minerals from the raw clays and the new phases formed during firing, researchers have identified various secondary phases that crystallized after firing. These were related both to the transformation of such new phases and to the precipitation in the pores of chemical elements dissolved in aqueous solutions (Maritan, 2020). Zeolites and calcite – resulting from recarbonation, precipitation and/or the alteration of gehlenite – occur frequently as post-firing (i.e., secondary) mineral phases in Ca-rich ceramic bodies (Buxeda i Garrigos and Cau Ontiveros, 1995; Buxeda i Garrigos et al., 2002; Fabbri et al., 2014).

Multi-analytic studies of ancient bricks offer interesting insights into the transformations that took place within the ceramic bodies during or after firing and shed light on the manufacturing processes. In Padua, fired bricks have been widely used as a building material throughout the city's long history, and the most representative are typically yellow or beige in color. In previous research on this most representative type of brick, Pérez-Monserrat et al. (2021, 2022) found that (i) they were produced with highly calcareous raw clays that were quite rich in magnesium; (ii) they show abundant Ca- and Mg-rich high-temperature phases as well as secondary calcite and zeolite hydration products; (iii) they display good mechanical behavior and resistance to frost and salt crystallization action; and (iv) they are in a good state of conservation, especially those laid in areas subject to high levels of humidity. On the basis of these studies, a range of different bricks from historic constructions in the city are analyzed in this paper. The main aims of this research are (i) to carry out a detailed compositional and microstructural analysis of this representative type of brick in order to understand the formation mechanism of both the high-temperature phases and the secondary phases and (ii) to identify the production technologies that may have brought about the transformations that took place within these yellow- and beige-colored bricks.

Brief introduction to the geology and the climate in the province of Padua

Padua's central location in the Veneto region (northeastern Italy) and its numerous waterways fostered the development of the area, which has been a strategic region for trade since Roman times. The province of Padua is located on the eastern side of the Po Plain, which is mainly covered by Pleistocene and Holocene fluvio-glacial deposits. The fact that there are virtually no rocky outcrops in the vicinity and the abundant availability of raw clays have historically favored the use of fired bricks as the main building material in the city. The only nearby rock outcrops are in the Euganean Hills, from which trachyte and rhyolite have traditionally been extracted for construction purposes (Germinario et al., 2017).

The city of Padua was built on top of Quaternary alluvial deposits from the Brenta and Bacchiglione rivers. The sand fraction from these deposits contains, above all, silicates and carbonates (calcite and dolomite) as well as metamorphic and volcanic rock fragments, while the clay fraction consists mainly of montmorillonite, illite–montmorillonite, chlorite, illite and kaolinite (Jobstraibitzer and Malesani, 1973). Carbonate leaching and reprecipitation within the clayey sediments comprise a frequent pedogenic process in the formation of the soils near the city (Cucato et al., 2008), yielding impure carbonate fragments aggregated with clay materials and/or clayey grains cemented by carbonates. This leaching and precipitation of carbonates, together with alternating oxidizing and reducing conditions during the Pleistocene–Holocene, resulted in the formation of calcic horizons, characterized by the accumulation of $CaCO_3$ in nodules and crusts. They also gave rise to a calcic paleosol that represents a subsurface layer known in the region as *caranto* (Mozzi et al., 2003; Donnici et al., 2011). These sedimentological processes yielded calcareous-rich groundwaters and surface runoff in the area. In addition to the carbonate-rich clays, widely present in the alluvial deposits around the city of Padua (Maritan, 2004), the alteration of the nearby volcanic rocks, especially the trachyte, gave rise to important deposits of Fe-rich clays (Cucato et al., 2008).

In the province of Padua, the climate is warm and temperate. The summers are hot and humid, while the winters are very cold, and it is partly cloudy all year round. There is significant rainfall throughout the year, with an annual average of circa 1000 mm. The average temperature is 15 °C and the average annual relative humidity is 74 % (Agenzia Regionale per la Prevenzione e Protezione Ambientale del Veneto, ARPAV; https://www.arpa.veneto.it/dati-ambientali/open-data/clima/principali-variabili-meteorologiche, last access: 14 November 2021).

2 Methodology

Forty fired bricks were sampled (taking fragments or entire bricks) from four emblematic constructions in the city of Padua: (i) the Basilica of Saint Justine (fifth/sixth–sixteenth centuries), from the early Christian (fifth–sixth centuries) and Romanesque (twelfth–thirteenth centuries) periods; (ii) the Elderly Tower (thirteenth century); (iii) the tower of the old castle of the Carraresi family, nowadays known as La Specola (fourteenth century); and (iv) the Renaissance walls (sixteenth century, samples were taken from various different sections of the perimeter). Overall, the bricks were in a good state of conservation. One-half were yellow or beige, and the other half were reddish, orange or brown (Table 1). On a freshly cut surface, some of the yellow and beige bricks displayed fine- and medium-grained inclusions within a compact, uniform matrix. Other samples, including the pale-red-colored and orange-colored bricks, showed large numbers of particles with very heterogeneous sizes. These were mainly lumps of clay and carbonate inclusions, contained within a matrix with a flowing texture, corresponding in turn to Fe-rich and carbonate clay materials. A few rounded or irregularly shaped pores were noted, some of which were partially filled by crystals.

The brick surface color was measured by spectrophotometry, using a portable 3nh NS800 spectrophotometer. On a circular measurement area of 8 mm diameter, a D65 standard light source and 10° viewing angle were selected. The UNE-EN 15886 (2011) standard was followed, and the CIELAB and CIELCh color spaces were used. The parameters measured were lightness (L^*), with values ranging from 0 (pure black) to 100 (pure white); chromatic coordinates a^* (+60 is red; −60 is green) and b^* (+60 is yellow; −60 is blue); chroma (C^*) or color saturation, ranging from 0 (dullness) to 100 (vividness); and the hue angle (h^*) from 0 to 360°. Ten measurements per sample were taken on a freshly cut surface.

The chemistry of the ceramic bodies was analyzed by X-ray fluorescence (XRF) with an S2 Ranger EDXRF Bruker AXS spectrometer with a Pd X-ray generator. The working conditions were 50 kV, 2 mA and 50 W. Major and minor oxides were determined on pressed pellets. Prior to the analysis, 7 g per sample was ground to powder in an agate mortar. Loss on ignition was determined gravimetrically as the weight loss recorded between 110 and 1000 °C.

The mineral phases in the samples were identified by X-ray powder diffraction (XRPD), using a PANalytical X'Pert PRO diffractometer in Bragg–Brentano geometry equipped with a Co X-ray tube and an X'Celerator detector. The results were interpreted with the X'Pert HighScore Plus software. The bricks were examined in thin sections by polarized-light optical microscopy (POM), using a Nikon Eclipse E660 microscope equipped with a Canon 650 digital camera and the Canon EOS digital microphotography system.

The microstructural features of the samples were described in detail by high-resolution scanning electron microscopy (HRSEM), using a Carl Zeiss STM (AURIGA series) and microanalysis by means of energy-dispersive X-ray spectroscopy (EDS). Fragments and polished thin sections coated with graphite were observed in back-scattered electron (BSE) and secondary electron (SE) mode.

3 Results

3.1 Chemical and mineralogical composition

On the basis of the chemical composition, all the samples are rich in CaO (> 5 %) and are plotted in the carbonate-rich area of the ternary diagram SiO_2–Al_2O_3–CaO (Fig. 1a), with the exception of brick RW_11, which has the lowest CaO content. Two main clusters were identified, lying adjacently to one another (Fig. 1a). When MgO content was also considered, a sharper division was observed: carbonatic bodies (CBs), with CaO + MgO percentages in the range 15 %–25 % (almost 25 % of the samples), and carbonatic-high carbonatic bodies (CHCBs), with CaO + MgO percentages in the range 27 %–38 % (comprising 75 % of the bricks) (Fig. 1b). While the CHCB samples have quite similar composition, forming quite a tight, compact group, the CB samples show much greater compositional variability and are highly scattered when the ternary system CaO–Fe_2O_3–MgO is considered (Fig. 1d). Taking into account pure Ca-aluminosilicate and calcium-/magnesium-silicate phases, the CHCB samples display a chemical composition that is plotted between wollastonite ($CaSiO_3$)/diopside ($CaMgSi_2O_6$) and melilite (general formula $Ca_2(Mg,Al)(Al,Si)SiO_7$) (Fig. 1b), with slightly lower calcium and/or magnesium oxides contents and higher aluminum contents, and/or between wollastonite and diopside (Fig. 1c), although in general they show a higher silica content.

The mineral phases detected by XRPD – relict components of the base clays, new (during firing) and secondary (post-firing) phases – are shown in Table 2. Two main mineral assemblages were detected in the samples belonging to the CB and CHCB groups: (i) high content in relict components (overall quartz, illite and primary calcite) and very few high-temperature phases (sub-groups CB_1 and $CHCB_1$) and (ii) fewer relict minerals – almost no illite – and quite abundant newly formed phases (sub-groups CB_2 and $CHCB_2$). Hematite was detected in some samples belonging to the CB_2 sub-group, and forsterite was detected in small quantities in some of the $CHCB_2$ samples. As regards the secondary phases, calcite was identified in many CB_2 and $CHCB_2$ samples (and was especially significant in the latter), although the distinction of secondary calcite from possible relict calcite should be performed by microscopic and microstructural description. Important concentrations of analcime were present

Table 1. List of the samples taken, their main textural features and colorimetric parameters measured on a freshly cut surface. Abbreviations: CL, clay lumps; CI, carbonate inclusions; FT, flowing texture; +, slightly; ++, quite; +++, very; −, not observed.

Construction	Date	Sample	Textural features					Color (CIELAB and CIELCh)					
			Matrix	CL	CI	FT	Porosity	Hue	L^*	a^*	b^*	C^*	h^*
Basilica of Saint Justine (SJ), 5th/6th–16th centuries	5th–6th centuries	SJ_1	Uneven +	+	−	+	Rounded +	Pale red	63.0	12.0	20.9	24.1	60.0
		SJ_2	Uneven +	+++	+	++	−	Red	54.6	16.7	21.9	27.5	52.8
		SJ_3	Uneven +	++	−	+	−	Yellow	69.7	7.0	17.6	18.9	68.2
		SJ_4	Even +++	−	−	−	Elongated ++	Yellow	77.3	0.8	20.4	20.4	87.9
	12th–13th centuries	SJ_5	Even +++	−	−	−	Rounded +	Yellow	68.6	3.9	29.2	29.4	82.3
		SJ_6	Even +++	−	−	−	Rounded +	Yellow	74.3	1.2	19.6	19.6	86.6
		SJ_7	Uneven +	++	−	+	Elongated +	Orange	59.5	13.9	23.2	27.0	59.1
		SJ_8	Uneven +++	+++	++	−	Rounded +	Beige	68.5	8.9	21.1	22.9	67.2
Elderly Tower (ET), 13th century		ET_1	Even +++	+++	−	−	Rounded +	Beige	64.7	8.4	17.9	20.3	64.0
		ET_2	Uneven +	++	++	++	Irregular +	Beige	63.5	13.2	21.2	25.0	58.5
		ET_3	Uneven +++	+++	+++	−	Irregular +	Orange	64.3	11.8	19.0	22.4	58.2
		ET_4	Even ++	+	−	−	Rounded +	Yellow	70.8	5.8	22.3	23.1	75.4
Tower of the old castle of the Carraresi family, La Specola (SP), 14th century		SP_1	Even +++	+	−	−	−	Beige	68.5	10.5	22.3	24.1	70.2
		SP_2	Uneven ++	+++	+	−	Irregular +	Pale red	61.2	12.6	19.2	23.0	56.8
		SP_3	Uneven +++	+++	++	++	Irregular +	Red	58.2	13.2	20.4	24.3	57.2
		SP_4	Uneven +++	+++	++	++	Irregular +	Red	47.3	14.6	20.9	21.9	56.5
		SP_5	Even +++	−	−	−	Irregular +	Yellow	63.8	12.8	22.3	25.4	61.4
Renaissance walls (RW), 16th century		RW_1	Even +++	−	−	−	−	Brown	57.9	14.0	20.6	24.9	55.8
		RW_2	Even ++	+	−	+	Irregular +	Yellow	67.0	7.8	22.6	23.9	71.0
		RW_3	Uneven +	+++	−	−	Irregular +	Pale red	59.9	13.9	19.5	24.0	54.5
		RW_4	Even ++	+	+++	−	Irregular +	Beige	66.5	8.7	18.9	20.8	65.3
		RW_5	Even +++	+	−	−	Irregular +	Orange	60.3	13.4	20.6	24.5	56.9
		RW_6	Uneven +++	+++	++	+	Irregular ++	Beige	63.7	9.0	20.8	22.7	66.5
		RW_7	Uneven +++	++	+	+++	−	Beige	61.7	11.0	20.2	23.0	61.4
		RW_8	Uneven +	++	−	+	Irregular +	Beige	63.5	7.5	21.7	23.0	70.9
		RW_9	Uneven +	++	−	−	Irregular +	Brown	58.1	12.6	21.4	24.9	59.7
		RW_10	Uneven ++	+++	−	++	Rounded ++	Beige	66.3	8.8	22.2	23.9	68.3
		RW_11	Uneven ++	++	−	+++	Rounded ++	Dark red	46.5	8.3	11.6	14.3	53.9
		RW_12	Uneven +++	+++	+	++	Rounded ++	Brown	53.2	8.4	19.1	20.9	66.2
		RW_13	Even +++	+	−	−	−	Orange	56.4	17.7	25.6	31.1	55.4
		RW_14	Uneven ++	++	−	+++	−	Orange	59.4	15.7	24.0	28.7	56.8
		RW_15	Uneven +++	+++	+++	+++	Rounded +	Beige	68.5	10.7	22.1	24.6	64.2
		RW_16	Even ++	+	−	−	Irregular +	Pale red	61.7	11.9	18.9	22.4	58.0
		RW_17	Uneven +++	+++	+++	+++	Rounded +	Beige	63.6	9.9	21.7	23.8	65.6
		RW_18	Even ++	+	++	+	Irregular +	Beige	69.5	8.1	21.1	22.6	69.1
		RW_19	Even ++	+	+	−	Irregular +	Pale red	63.2	14.1	21.7	25.9	57.0
		RW_20	Uneven +	+	+	+	Rounded +	Brown	55.2	9.1	20.1	22.0	65.6
		RW_21	Uneven +++	+++	+++	+++	Rounded +	Beige	65.9	10.8	19.3	22.1	60.9
		RW_22	Even ++	++	−	−	Irregular +	Dark orange	53.0	20.4	30.2	36.4	55.9
		RW_23	Even +++	+	+	−	Irregular +	Dark orange	58.6	15.9	23.3	28.2	55.7

in some $CHCB_2$ samples, and aragonite and gypsum were detected in some of the samples from both groups.

In chemical terms, the ceramic bodies are moderately rich in SiO_2 and display high quantities of Al_2O_3 and Fe_2O_3, limited amounts of K_2O and Na_2O, a quite significant MgO content, and a very high concentration of CaO (Table 3). The CB bricks have higher average SiO_2, Al_2O_3, Fe_2O_3, K_2O and Na_2O contents than the CHCB bricks (SiO_2 is 46.2 wt %–40.3 wt %; Al_2O_3 is 17.1 wt %–14.1 wt %; Fe_2O_3 is 6.7 wt %–5.7 wt %; Na_2O is 1.6 wt %–1.5 wt %), while the combined total for CaO and MgO is lower (CaO + MgO is 17.5 wt %–24.8 wt %). As observed in Fig. 1, the CBs show greater variability in terms of composition, especially regarding the amounts of SiO_2 and CaO, with values ranging from 35.8 wt % to 56 wt % (SD = 6.22) and from 4.4 wt % to 19.6 wt % (SD = 4.7), respectively. Within the sub-groups identified by XRPD analysis (Table 2), few differences were observed between the average data achieved by XRF (Table 3), except that the SiO_2 and Na_2O values were higher in the samples belonging to the CB_2 and $CHCB_2$ sub-groups (SiO_2 is 46.2 wt % and 41.4 wt %; Na_2O is 1.70 wt % and 1.6 wt %), respectively. The CB samples were found to have higher Fe_2O_3 contents (6.9 wt % in CB_1 and 6.5 wt % in CB_2). This was mainly due to the high illite content detected, although it could also suggest the use of chlorite clays. Samples with lower SiO_2/Al_2O_3 (S/A) ratios (S/A < 2.5) indicate a predominance of clay minerals over quartz. This may be due to the fact that the sediments are richer in clay than in sand. The higher SiO_2 and Al_2O_3 values in the CB samples indicate larger amounts of quartz and feldspar in the raw

Table 2. Mineralogical associations detected by XRPD analysis of the brick samples. Mineral abbreviations after Warr (2021): quartz (Qz); K-feldspars (Kfs); albite (Ab); illite (Ilt); calcite (Cal); gehlenite (Gh); diopside (Di); anorthite (An); forsterite (Fo); hematite (Hem); aragonite (Arg); analcime (Anl); gypsum (Gp). Secondary calcite (Cal (2nd)) was estimated on the basis of microscopic analysis. +: detected; ++: noticeable; +++: abundant; ++++: very abundant; −: not detected.

	Pristine phases					Firing phases					Secondary phases			
	Qz	Kfs	Ab	Ilt	Cal (1st)[a]	Gh[b]	Di	An	Fo	Hem	Cal (2nd)[a]	Arg	Anl	Gp
Carbonatic bodies (CBs), 10 samples														
CB_1, firing temperatures circa of 800 °C														
SP_2	+++	−	+	++	++	+	−	−	−	−	−	++	−	−
RW_9	++++	+	++	++++	+++	−	−	−	−	−	−	−	−	−
RW_13	+++	+	++	++++	++	−	−	−	−	−	−	−	−	+++
RW_22	++++	+	++++	++	+++	−	−	−	−	−	−	−	−	−
CB_2, firing temperatures from 900 to over 950 °C														
SJ_2	++++	++++	−	−	−	−	−	++	−	++	+	−	−	+
SJ_4	+	+	−	−	−	+	+++	++	−	−	++	−	−	−
SP_1	++	++	−	−	−	−	+++	++++	−	−	+	−	++	−
SP_4	++++	+++	−	+	−	−	+	++	−	++	++	−	−	−
RW_11[c]	++++	+	++	−	−	−	−	−	−	+++	−	−	−	−
RW_20	++++	−	−	−	−	+	++	++++	−	−	−	+	−	−
Carbonatic-high carbonatic bodies (CHCBs), 30 samples														
$CHCB_1$, firing temperatures circa of 800 °C														
SJ_1	++++	+	−	+	++	−	+	+	−	−	−	++	−	+
SJ_7	++++	−	+	+++	++++	−	−	−	−	−	−	−	−	+
SP_5	++++	−	+	++	+	−	−	−	−	−	−	++	−	−
RW_1	++++	+	+	++	++	−	−	−	−	−	−	−	−	+
RW_5	++++	++	++	++++	++	−	−	−	−	−	−	−	−	+
RW_14	++++	+	+	+++	+	−	−	−	−	−	−	+	−	+
RW_23	++++	+	+	+++	++++	−	−	−	−	−	−	−	−	+
$CHCB_2$, firing temperatures from 900 to over 950 °C														
SJ_3	++++	−	−	−	−	+++	++	+++	+	−	+	−	+	−
SJ_5	++	−	−	−	−	+	++++	++++	+	−	+	−	+++	+
SJ_6	+	−	−	−	−	+++	++++	+++	+	−	+++	−	+++	−
SJ_8	++++	++	−	−	−	++++	+++	++	−	−	+	++	−	−
ET_1[c]	++++	++	−	−	−	++++	++++	++	+	−	+	−	+	−
ET_2	++++	+++	−	−	−	++	++++	++	−	−	++++	−	−	−
ET_3	++++	++	−	+	−	+	+	++	−	−	++++	++	−	−
ET_4	+++	−	−	−	−	++++	++++	+++	+	−	++++	−	+++	−
SP_3	++++	−	−	−	−	−	++	+++	−	−	−	−	−	−
RW_2	+++	−	−	−	−	++++	++++	+++	+	−	+++	++	++	−
RW_3[c]	++++	+++	−	+	−	−	++	++	−	−	++	+	−	−
RW_4	++++	+++	−	−	−	+++	++++	+++	−	−	++++	−	−	−
RW_6	++++	++	−	−	−	++	++++	+++	+	−	++++	−	−	−
RW_7	++++	++	−	−	−	+++	+++	+++	−	−	++++	−	−	−
RW_8	++++	−	−	−	−	+	++++	++++	+	−	++++	−	−	−
RW_10	++++	+++	−	−	−	++	++++	+++	+	−	−	+	−	−
RW_12	++++	−	−	−	−	+	++++	++++	−	−	++	−	−	−
RW_15	++++	++	−	−	−	+	++++	+++	+	−	+++	−	−	−
RW_16	++++	+++	−	+	−	+	+	+	−	−	++++	−	−	−
RW_17	++++	−	−	−	−	+++	++++	+++	−	−	++++	−	−	−
RW_18	++++	+++	−	−	−	++	++++	+++	+	−	++++	++	++	−
RW_19	++++	++	−	−	−	++++	+	++	−	−	++++	−	−	−
RW_21	++++	+++	−	−	−	+++	+	++	−	−	++++	−	−	−

[a] Although based on mineral assemblage, the assignment of primary or secondary calcite by XRPD should be carefully analyzed. [b] Corresponding to an intermediate melilitic compound between the solid-solution end-members åkermanite and gehlenite. [c] Spinel was also detected in RW_11 and chabazite (zeolite group mineral) in ET_1 (+) and RW_3 (++).

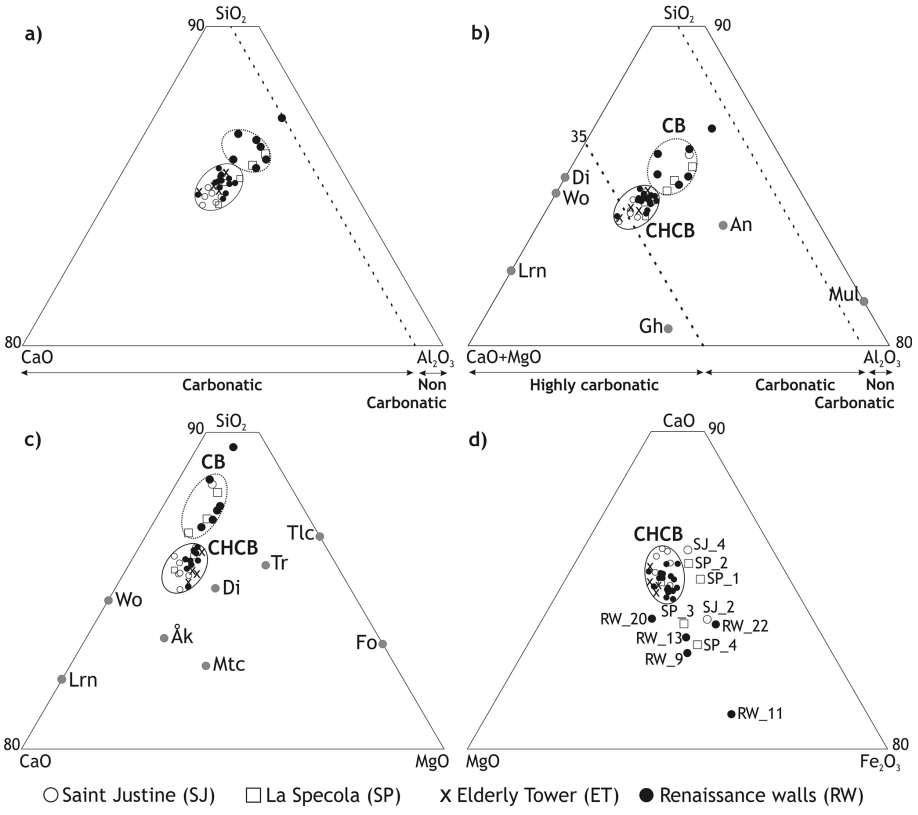

Figure 1. Plotting of the chemical composition of bricks in ternary diagrams. The samples are plotted within the carbonatic body (CB) and carbonatic-high carbonatic body (CHCB) groups (except RW_11). See Tables 2 and 3 for entire sample numbering. Panels **(a)** and **(b)** are adapted from Gliozzo (2020) and **(c)** from Trindade et al. (2009). Mineral abbreviations after Warr (2021): åkermanite (Åk), anorthite (An), diopside (Di), forsterite (Fo), gehlenite (Gh), larnite (Lrn), monticellite (Mtc), mullite (Mul), talc (Tlc), tremolite (Tr) and wollastonite (Wo).

clays, while the higher K_2O/Na_2O (K/N) ratios (K/N average is 2.34) indicate a higher illite content.

The high CaO+MgO content (over 13 wt % in almost all CB samples and over 22 wt % in nearly all the CHCB samples) could be due to the widespread formation of Ca-/Mg-rich mineral phases during firing and to the abundance of carbonates – from the raw clays and/or in the form of secondary carbonates. The decomposition of carbonates (of primary and/or secondary origin) and dihydroxylation of phyllosilicates cause an increase in loss-on-ignition (LOI) content. Both these processes produce highly reactive bodies during firing. The samples belonging to the CB_1 and $CHCB_1$ subgroups had higher overall LOI values (average of 9.42 wt % and 14.4 wt %, respectively). This seems to be related to the high content in illite, a mineral that is almost absent in the CB_2 and $CHCB_2$ samples (Table 2). High CaO and MgO contents indicate that the clay paste was rich in calcite and dolomite. However, since the bricks were fired at different temperatures and part of the calcite detected probably corresponds to secondary calcite, it is rather difficult to establish a relationship between the CaO + MgO and LOI values.

The chemical data obtained indicated that the brickmakers used silica-rich clays with considerable amounts of Ca carbonate, Mg carbonate and clay minerals. They also suggest the use of at least two compositionally different raw clays and/or two different recipes for preparing the ceramic pastes (mixtures of various different raw clays), one rich in silica and iron and the other with a high carbonate content.

Even though the yellow (positive b^* values) and red (positive a^* values) shades are directly related to the CaO and Fe_2O_3 contents, respectively (Klaarenbeek, 1961; Nodari et al., 2007), the chromatic grouping of the bricks was not as clearly defined as the classification based on chemical composition. In fact, when the chromatic coordinates a^* and b^* were analyzed, many samples belonging to the CB and CHCB clusters grouped quite closely together (Fig. 2a, within the rectangular area). The coordinate a^* values for this joint group (rectangular area, of both CB and CHCB samples) were between 5 and 17 and the b^* values between 17 and 24, and there was more variability in the red component (a^*) than in the yellow one (b^*). Nearly all the CHCB samples were concentrated in this joint group, whereas the CB samples were more scattered (Fig. 2a).

A clearer distinction between the CB and CHCB groups can be observed when their chromatic values are compared with their CaO, CaO + MgO and Fe_2O_3 contents by means

Table 3. Chemical composition of the major and minor oxides (in wt %) of CB and CHCB bricks determined by XRF. Maximum, minimum, average and standard deviation values of the samples belonging to both groups are also shown. Abbreviations: S/A, SiO_4/Al_2O_3; K/N, K_2O/Na_2O; R_2O, $K_2O + Na_2O$; C + M, CaO + MgO; LOI, loss on ignition. The total amount also includes small amounts of SO_3, TiO_2, Cl^-, P_2O_5 and MnO oxides (wt %), which were also calculated but were not included in Table 3.

	SiO_2	CaO	Al_2O_3	MgO	Fe_2O_3	K_2O	Na_2O	S/A	K/N	R_2O	C + M	LOI	Total
Carbonatic bodies (CBs): sub-group CB_1													
SP_2	35.8	18.7	15.0	5.42	6.61	3.13	1.14	2.38	2.75	4.27	24.1	12.6	98.4
RW_9	42.2	8.95	17.8	6.11	6.89	4.09	1.06	2.37	3.84	5.15	15.1	11.4	98.5
RW_13	42.5	11.2	17.7	6.55	7.52	3.93	< 0.01	2.40	–	3.93	17.7	7.79	97.3
RW_22	50.8	9.44	16.9	3.77	6.66	3.27	1.79	3.01	1.83	5.05	13.2	5.88	98.5
Average	42.8	12.1	16.9	5.46	6.92	3.61	1.33	2.54	2.81	4.60	17.5	9.42	
SD	6.15	4.52	1.30	1.22	0.42	0.48	0.40	0.31	1.01	0.60	4.76	3.12	
Carbonatic bodies (CBs): sub-group CB_2													
SJ_2	50.0	9.52	17.7	4.10	6.32	3.31	1.72	2.83	1.93	5.03	13.6	4.59	97.2
SJ_4	41.2	19.6	16.2	4.90	6.12	3.36	1.41	2.54	2.37	4.77	24.5	5.77	98.5
SP_1	43.1	15.6	17.6	4.67	7.05	3.31	2.10	2.46	1.58	5.41	20.3	4.73	98.2
SP_4	47.6	9.19	19.0	5.29	6.86	3.90	1.42	2.51	2.75	5.32	14.5	5.64	98.9
RW_11	56.0	4.43	19.0	4.13	7.41	4.34	1.67	2.94	2.59	6.01	8.57	1.75	98.8
RW_20	52.7	12.1	13.8	7.68	5.23	2.62	1.85	3.81	1.42	4.47	19.8	2.79	98.9
Average	48.4	11.7	17.2	5.13	6.50	3.47	1.70	2.85	2.11	5.17	16.9	4.21	
SD	5.15	4.86	1.80	1.21	0.71	0.54	0.24	0.46	0.50	0.49	5.22	1.47	
Average CB	46.2	11.9	17.1	5.26	6.67	3.53	1.57	2.72	2.34	4.94	17.1	6.30	
SD CB	6.22	4.7	1.64	1.23	0.67	0.52	0.34	0.45	0.75	0.60	5.09	3.45	
	SiO_2	CaO	Al_2O_3	MgO	Fe_2O_3	K_2O	Na_2O	S/A	K/N	R_2O	C + M	LOI	Total
Carbonatic-high carbonatic bodies (CHCBs): sub-group $CHCB_1$													
SJ_1	32.2	18.9	11.5	7.12	4.57	2.71	1.15	2.79	2.36	3.86	26.0	18.1	96.3
SJ_7	34.6	17.9	13.7	6.25	5.31	2.85	0.99	2.53	2.89	3.73	24.2	17.7	99.3
SP_5	37.4	15.6	13.5	6.79	5.23	2.96	1.38	2.77	2.16	4.13	22.4	14.1	97.0
RW_1	37.8	15.4	14.5	6.75	5.70	3.10	1.03	2.61	3.03	4.13	22.1	14.7	98.8
RW_5	39.4	15.4	14.3	7.37	6.08	2.95	1.05	2.76	2.80	4.27	22.7	12.2	98.7
RW_14	37.8	17.1	15.1	7.44	6.34	3.38	1.25	2.50	2.69	4.49	24.5	10.4	98.8
RW_23	36.0	17.4	15.0	6.73	6.32	2.90	0.95	2.41	3.05	5.50	24.1	13.7	99.0
Average	36.5	16.8	13.9	6.92	5.65	2.98	1.11	2.62	2.71	4.30	23.7	14.4	
SD	2.41	1.38	1.23	0.42	0.65	0.21	0.15	0.15	0.34	0.58	1.39	2.77	
Carbonatic-high carbonatic bodies (CHCBs): sub-group $CHCB_2$													
SJ_3	43.2	16.5	14.0	7.22	6.17	2.98	1.30	3.10	2.30	3.58	23.7	7.59	98.9
SJ_5	42.0	20.3	13.1	6.42	5.16	1.55	2.79	3.20	0.56	3.61	26.7	6.93	98.2
SJ_6	39.4	20.9	13.1	6.83	4.94	1.88	2.28	3.00	0.82	3.61	27.7	8.91	98.2
SJ_8	38.5	19.3	13.6	8.22	5.29	2.77	1.45	2.84	1.92	3.84	27.5	9.66	98.8
ET_1	41.9	19.6	14.1	9.45	5.75	2.74	1.83	2.98	1.49	3.85	29.0	3.67	99.0
ET_2	42.8	16.1	14.2	8.00	5.44	2.91	1.47	3.02	1.98	3.96	24.1	8.14	99.0
ET_3	36.1	16.8	13.5	7.74	5.43	3.87	1.63	2.68	2.37	4.00	24.5	14.1	99.1
ET_4	38.6	21.0	12.0	9.04	5.34	2.12	2.01	3.22	1.05	4.07	30.1	8.65	98.8
SP_3	45.0	12.1	17.8	6.33	6.88	3.49	1.61	2.52	2.17	4.09	18.5	5.59	98.8
RW_2	38.2	20.9	11.8	9.21	5.30	1.99	1.63	3.22	1.22	4.15	30.1	9.70	98.8
RW_3	40.0	15.3	14.6	6.77	5.83	3.28	0.79	2.74	4.14	4.22	22.1	12.1	98.7
RW_4	42.9	17.1	14.0	7.34	5.27	2.40	1.56	3.07	1.54	4.24	24.4	8.25	98.8
RW_6	42.6	17.3	14.0	7.28	5.47	2.93	1.57	3.05	1.87	4.29	24.6	7.94	99.0
RW_7	41.8	17.5	14.5	6.72	5.95	2.82	1.47	2.88	1.91	4.34	24.2	8.01	98.8
RW_8	44.2	16.9	13.1	8.11	5.44	2.66	1.59	3.37	1.68	4.34	25.1	6.82	98.8
RW_10	42.6	17.8	13.9	8.55	5.70	2.85	1.69	3.06	1.68	4.35	26.4	6.11	99.2
RW_12	47.8	15.0	14.9	6.86	6.41	2.85	1.64	3.21	1.74	4.38	21.9	3.36	98.8
RW_15	42.2	16.3	16.6	7.07	6.45	2.98	1.60	2.54	1.86	4.50	23.4	5.76	98.9
RW_16	40.3	17.6	13.6	7.21	5.43	2.27	1.34	2.98	1.70	4.54	24.8	11.0	98.8
RW_17	42.3	16.9	16.2	6.90	6.75	2.83	1.51	2.62	1.87	4.57	23.8	5.56	99.0
RW_18	40.8	18.5	14.8	6.55	5.43	2.63	1.46	2.75	1.81	4.58	25.0	8.91	99.0
RW_19	39.2	18.0	16.1	5.92	5.90	2.57	1.17	2.44	2.20	4.63	23.9	10.2	99.1
RW_21	40.4	18.1	13.3	7.40	5.27	2.33	1.25	3.04	1.86	5.09	25.5	10.8	98.9
Average	41.4	17.6	14.2	7.44	5.70	2.68	1.59	2.94	1.81	4.21	25.1	8.16	
SD	2.54	2.11	1.41	0.95	0.52	0.52	0.39	0.25	0.67	0.37	2.66	2.58	
Average CHCB	40.3	17.4	14.1	7.32	5.68	2.75	1.48	2.86	2.02	4.23	24.8	9.63	
SD CHCB	3.26	1.97	1.35	0.88	0.54	0.48	0.40	0.27	0.72	0.42	2.48	3.72	

of principal component analysis (PCA; Fig. 2b). In this case, the CHCB samples are more closely concentrated together than the CB samples and there is almost no overlap between the two groups. This suggests that the red and yellow colors of these bricks depend above all on their CaO, CaO + MgO and Fe_2O_3 contents, although the color-based grouping was not as clearly defined as that based on chemical composition, as mentioned earlier. In fact, when the results reported in Tables 1 and 3 are compared, it is observed that the yellow, beige and orange bricks belonged mainly to the CHCB group, while the red and brown ones belonged to the CB group. A higher chromatic variability was found in the latter group, in line with its higher chemical variability.

The mineral phases identified by XRPD (Table 2) provide information on the firing dynamics. This shows for example that the chemical reaction of illite/muscovite dehydroxylation (Reaction R1) occurs between 450 and 780 °C (Wang et al., 2017), and the dehydroxylated phase remains almost unchanged up to 850–950 °C (Aras, 2004; Khalfaoui et al., 2009) as follows:

$$KAl_2(Si_3Al)O_{10}(OH)_2 \text{ muscovite} \rightarrow H_2O + KAl_2(Si_3Al)O_{11} \text{ dehydroxylated phase} \quad (\Delta_rH^0 = 371\,kJ\,mol^{-1}). \quad (R1)$$

In pure systems and/or if pure crystals of calcite and dolomite are considered, carbonate decomposition begins quite early, at about 500 °C for dolomite (Rodriguez-Navarro et al., 2009, 2012). Thermal decomposition of calcite is completed at around 800–850 °C (Iordanidis et al., 2009), and dolomite decomposition yields calcite and periclase (Reaction R2). Lime is released from calcite decarbonation up to 900 °C (Reaction R3), and the end products are basically MgO and CaO, both of which are highly active. In addition, as lime recarbonates faster than periclase (Webb, 1952), lime recarbonates during firing, only to decompose again as the temperature increases. This occurs as follows:

$$CaMg(CO_3)_2 \text{ dolomite} \rightarrow CaCO_3 \text{ calcite} + MgO \text{ periclase} + CO_2 \quad (\Delta_rH^0 = 122\,kJ\,mol^{-1}), \quad (R2)$$

$$CaCO_3\ calcite \rightarrow CaO \text{ lime} + CO_2 \quad (\Delta_rH^0 = 179\,kJ\,mol^{-1}). \quad (R3)$$

Gehlenite is formed at about 800–850 °C (Cultrone et al., 2001) from two different main reactions – (i) when lime reacts with free silica and alumina derived from the dehydroxylation of illite (Reaction R4) and (ii) when K-feldspar reacts with calcite (Reaction R5) – as follows:

$$2KAl_2(Si_3Al)O_{10}(OH)_2 \text{ illite} + 6CaCO_3 \text{ calcite} \rightarrow 3Ca_2Al_2SiO_7 \text{ gehlenite} + 3SiO_2 + K_2O + 2H_2O + 6CO_2 \quad (\Delta_rH^0 = 518\,kJ\,mol^{-1}), \quad (R4)$$

$$2KAlSi_3O_8 \text{ K-feldspar} + 2CaCO_3 \text{ calcite} \rightarrow Ca_2Al_2SiO_7 \text{ gehlenite} + 5SiO_2 + K_2O + 2CO_2 \quad (\Delta_rH^0 = 1041\,kJ\,mol^{-1}). \quad (R5)$$

The gehlenite detected corresponds to an intermediate compound of the solid-solution end-members. It falls somewhere between Mg-rich (åkermanite, $Ca_2MgSi_2O_7$) and Al-rich (gehlenite, $Ca_2Al_2SiO_7$), with a general formula of $Ca_2(Mg,Al)(Al,Si)SiO_7$ (melilite). Gehlenite normally behaves as an intermediate phase that reacts with quartz and alumina, thus giving rise to anorthite (Reaction R6) around 900 °C (Traoré et al., 2000; Riccardi et al., 1999). Anorthite may also be formed by the reaction of calcite both with quartz and K-feldspar (Reaction R7) (Elias and Cultrone, 2019) and with quartz and alumina (Reaction R8). Substantial anorthite contents suggest a firing temperature ≥ 900 °C (Daghmehchi et al., 2016), although the fine grain of the raw materials may enhance its crystallization at lower temperatures (Rathossi and Pontikes, 2010) as follows:

$$Ca_2Al_2SiO_7 \text{ gehlenite} + 3SiO_2 + Al_2O_3 \rightarrow 2CaAl_2Si_2O_8 \text{ anorthite} \quad (\Delta_rH^0 = -75\,kJ\,mol^{-1}), \quad (R6)$$

$$CaCO_3 \text{ calcite} + 2SiO_2 + 2KAlSi_3O_8 \text{ K-feldspar} \rightarrow CaAl_2Si_2O_8 \text{ anorthite} + K_2O + 6SiO_2 + CO_2 \quad (\Delta_rH^0 = 527\,kJ\,mol^{-1}), \quad (R7)$$

$$2Al_2O_3 \text{ alumina} + 4SiO_2 + 2CaCO_3 \text{ calcite} \rightarrow 2CaAl_2Si_2O_8 \text{ anorthite} + 2CO_2 \quad (\Delta_rH^0 = 153\,kJ\,mol^{-1}). \quad (R8)$$

At around 900 °C, diopside may be formed through the reaction between silica and dolomite (Reaction R9) (Cultrone et al., 2001):

$$CaMg(CO_3)_2 \text{ dolomite} + 2SiO_2 \text{ quartz} \rightarrow CaMgSi_2O_6 \text{ diopside} + 2CO_2 \quad (\Delta_rH^0 = 215\,kJ\,mol^{-1}). \quad (R9)$$

It is important to bear in mind that it is difficult to identify the specific clinopyroxene on the basis of the XRPD peaks (Dondi et al., 1998) and that although ceramic pyroxenes are generally referred to in the literature as diopside (Peters and Iberg, 1978; Shoval, 1988), in compositional terms the clinopyroxene could also correspond, for instance, to a fassaite (Dondi et al., 1998).

As the reactivity of lime is higher than that of periclase, the former is consumed faster. From the excess of periclase, Mg silicates like forsterite can nucleate as firing temperature

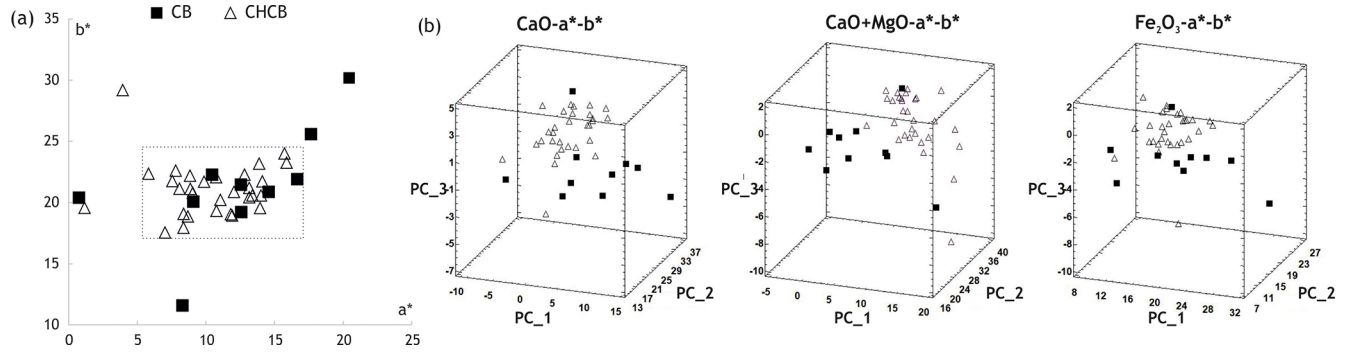

Figure 2. Chromatics of the CB and CHCB samples compared with their CaO, CaO + MgO and Fe_2O_3 contents. **(a)** Plotting of the chromatic coordinates a^* and b^* – many samples are closely grouped together within the rectangular area; **(b)** score plot of the principal component analysis (PCA). PC1, PC2 and PC3 were determined by taking into consideration the chromatic coordinates a^* and b^* and the CaO, CaO + MgO and Fe_2O_3 content, respectively.

rises, both at the expense of Ca–Mg silicates (Reaction R10) (Trindade et al., 2009) and by the reaction of periclase with silica (Reaction R11). These transformations occur via the following reactions:

$$\mathrm{CaMgSi_2O_6\ diopside + 3MgO\ periclase \rightarrow}$$
$$\mathrm{2Mg_2SiO_4\ forsterite + CaO\ lime}$$
$$(\Delta_r H^0 = 29\,\mathrm{kJ\,mol^{-1}}), \quad \text{(R10)}$$
$$\mathrm{SiO_2 + 2MgO\ periclase \rightarrow Mg_2SiO_4\ forsterite}$$
$$(\Delta_r H^0 = -59\,\mathrm{kJ\,mol^{-1}}). \quad \text{(R11)}$$

As periclase may also be formed after the decomposition of other Mg-rich minerals such as diopside, monticellite, åkermanite and/or forsterite (Trindade et al., 2009), there is an available supply of MgO almost throughout the whole firing process. Magnesium therefore seems to be the most widely involved element in the formation of the new phases in Mg-rich base clays, as was observed in previous research (Khalfaoui et al., 2006).

Well-crystallized hematite is a significant component only after heating at 900 °C (Trindade et al., 2009), although the firing of calcareous clays may lead to the formation of hematite at around 750–850 °C (Nodari et al., 2007; Tenconi et al., 2013). Hematite may also be generated by the dehydration of the pristine iron oxyhydroxides and the recrystallization of iron released during the breakdown of the phyllosilicates (Vedder and Wilkins, 1969). The entrapment of iron within the structure of gehlenite and Ca pyroxenes inhibits the formation of hematite, thereby reducing the red component of the ceramic pastes (Klaarenbeek, 1961). This suggests that hematite was only detected in the CB_2 samples because of the high firing temperatures and the lower carbonate content of the raw clays, which resulted in turn in lesser development of Ca-rich silicates that entrapped less iron, thus leaving more available to form hematite.

For the reactions reported above, the standard enthalpy of reaction ($\Delta_r H^0$) was calculated using the molar enthalpies for the formation of each phase ($\Delta_f H^0$) provided in the literature (Holland and Powel, 1998; Kiseleva et al., 1996; Madivate et al., 2004) as follows:

$$\Delta_r H^0 = \Sigma_{\text{products},\,p}\,\nu_p \Delta_f H^0{}_p - \Sigma_{\text{reactants, re}}\,\nu_{\text{re}} \Delta_f H^0{}_{\text{re}}\ ,$$

where ν_p and ν_{re} are the stoichiometric coefficients of each product p and reactant re. Although the reactions took place at higher temperatures than the standard conditions (values were not recalculated), $\Delta_r H^0$ allowed us to define whether a reaction was endothermic (positive value) or exothermic (negative value). In most cases, the enthalpy of reaction was positive, i.e., endothermic, thus indicating that the reactions occurred after a sufficient amount of energy had been supplied by heating during firing. Exothermic reactions were only observed in two cases (Reactions R6 and R11).

The mineral assemblages detected point to the use of Ca- and Mg-rich (calcareous) clays and Fe content in illitic clays, in concordance with the general composition of the base clays obtained from the chemical data. On the basis of the presence – and quantity – of phyllosilicates and newly formed phases, it is possible to estimate the approximate temperatures at which the samples were fired. The higher the illite concentrations – in line with the lower amounts of newly formed phases – the lower the firing temperatures. The samples with the largest amounts of illite were fired at less than 850 °C, while those containing anorthite and diopside were fired at over 900 °C. In the CB_1 and CHB_1 samples, the quite significant presence of illite and the almost complete absence of high-temperature phases suggest firing temperatures of around 800 °C. Despite the homogeneous scenario observed in the $CHCB_2$ samples, these must have been fired at different temperatures in line with the relative abundance of the newly formed silicates. Therefore, when abundant amounts of gehlenite are detected, this indicates firing temperatures of around 900 °C, whereas large amounts of diopside and anorthite indicate higher firing temperatures of over 950 °C. Even though CB_2 and $CHCB_2$ samples displayed very simi-

lar mineral assemblages, they must have been produced with different raw clays, given that some CB_2 samples had quite a significant hematite content, while it was not detected in any of the $CHCB_2$ samples.

Analcime (a zeolite group mineral) and calcite secondary phases were also detected in significant amounts. In previous research, zeolite was detected by XRPD as a secondary hydration product in other ancient bricks used in Padua, probably due to the city's high humidity and the use of calcite-rich clays (Pérez-Monserrat et al., 2021, 2022). The hydration of the abundant amorphous phase yielded by highly fired calcareous clays may foster the formation of zeolites (Buxeda et al., 2002; Schwedt et al., 2006; Maritan, 2020), as may the presence of alkaline fluids (Pacheco-Torgal et al., 2008). The glassy phase is unstable under certain weathering conditions, and, over time, its alteration yields to the leaching of potassium, which in turn can produce leucite ($KAlSi_2O_6$) precipitation. For its part, analcime ($Na(Si_2Al)O_6 \cdot H_2O$)) may crystallize from the altered amorphous phase and through reaction with free silica, via the uptake of sodium from the environment (Buxeda i Garrigos et al., 2002). Nevertheless, the noteworthy presence of aluminum and calcium in the brick samples suggests the formation of zeolites such as wairakite ($CaAl_2Si_4O_{12} \cdot 2H_2O$), which has a similar XRPD pattern to that of analcime, and chabazite-Ca ($((Ca_{0.5},Na,K)4[Al_4Si_8O_{24}] \cdot 12H_2O$). Furthermore, the Ca-rich micro-sites in the calcite inclusions could promote the nucleation of gehlenite (Heimann and Maggetti, 1981), and this phase might be transformed into wairakite (Reaction R12) by the leaching action of water over a long period of time (Fabbri et al., 2014) according to the following reaction:

$$4Ca_2Al_2SiO_7 + 18H_2O \rightarrow CaAl_2Si_4O_{12} \cdot 2H_2O + 7Ca(OH)_2 + 6Al(OH)_3\,. \quad \text{(R12)}$$

As pristine carbonates and newly formed silicates cannot theoretically appear together (Fabbri et al., 2014), the calcite detected in CB_2 and $CHCB_2$ samples must be of secondary origin. Nevertheless, the classification of calcite as primary or secondary on the basis of XRPD (Table 2) analysis should be confirmed by microstructural observations, as already stated. This is because pristine calcite may persist at over 900 °C within calcite-rich systems if the calcite grains are coarse and crystalline, under rapid heating rates, or if the soaking time is short (Shoval et al., 1993; Maggetti et al., 2011; Maritan et al., 2006). Consequently, relict calcite and newly formed phases may occur simultaneously if these kinetic and thermodynamic conditions apply. Moreover, the increase in the CO_2 partial pressure that takes place inside the kiln during the firing of calcareous-rich clays slows the reactions down and may result in the incomplete decomposition of carbonates, even at high temperatures (García-Labiano et al., 2002; Cultrone, 2022). Aragonite nucleation could be due to the samples having quite significant magnesium contents, which could lead to the crystallization of Mg calcite and aragonite (Sondi and Slovenec, 2003). It could also be formed due to the presence of surrounding humic acids (Sondi and Juracic, 2010; Maritan, 2020) after the bricks were laid.

3.2 Microstructure and microchemical composition

Considering that more than half of the bricks studied belonged to the $CHCB_2$ sub-group, a detailed microstructural and microchemical analysis of the $CHCB_2$ samples using the POM and high-resolution scanning electron microscopy (HRSEM) techniques was performed. The samples had a fine-grained microstructure in which inclusions were dispersed in a matrix with incipient vitrification (Fig. 3a), largely owing to the fact that carbonates hamper the sintering of bricks at high temperatures as silica, alumina, lime and periclase are involved in the newly formed phases (Everhart, 1957; Alia et al., 1999). This incipient level of vitrification created quite porous bricks. This higher level of porosity was itself due to the decarbonization of the high carbonate content in the pristine clay pastes (Toledo et al., 2004; Issi, 2012) and/or partially to the air bubbles that might have been trapped in the pastes during shaping (Fabbri et al., 2014).

The particles are represented mostly by pristine Ca- and/or Mg-rich microcrystalline clayey lumps (Fig. 3a), Ca-plagioclase crystals, phyllosilicate pseudomorphs, and Mg-rich dark particles with bright reaction rims (Fig. 3b), formed by the reaction between the partially decomposed grain and the surrounding silicate groundmass (Heimann and Maggetti, 1981). Although Reactions (R6), (R7) and (R8) express the formation of anorthite as firing temperature increases, these Ca-plagioclase crystals mainly correspond to pristine plagioclase that acquired an anorthite-like composition during firing (Cultrone et al., 2014). In fact, plagioclases, with compositions from albite to andesite, are very abundant mineral components of the sands from the Brenta and Bacchiglione rivers, and the calcium terms are rare (Jobstraibitzer and Malesani, 1973). Quartz and K-feldspar relict grains with phase transformations at the edges can also be observed. It is suggested the formation of intermediate members of the åkermanite–gehlenite series from illite (Cultrone and Carrillo, 2020), and the open oval-shaped mica pseudomorphs with vesicles indicate that high temperatures were reached (Fig. 3c and EDS results).

As regards the mineralogical and microstructural changes that took place during the firing of the $CHCB_2$ bricks, the main features observed are the nucleation of pyroxene-type crystals within a Ca-aluminosilicate amorphous phase (Fig. 3d–f) and the formation of magnesium-silicate crystals within the Mg-rich clayey grains (Fig. 4d–i). In addition, zeolite hydration products formed within the coarse calcite grains (Fig. 5d–f). Significant amounts of secondary calcite, both recarbonated through the matrix (Fig. 3b, g and h) and

precipitated both through the matrix (Fig. 3i) and within the porosity (Fig. 5g–m), were also observed.

3.3 Crystallization of pyroxenes from a Ca-aluminosilicate amorphous phase

High-magnification imaging analysis by HRSEM shows that, in many areas, inclusions are bound by an amorphous phase (Fig. 3d) observed under POM as compact and optically inactive portions (Fig. 3g). This phase largely consists of the intermediate compound of the solid solution between the åkermanite and gehlenite end-members detected by XRPD, and it has been described as a melilitic composition matrix in other yellow bricks from monuments in the city of Padua studied in previous research (Pérez-Monserrat et al., 2022). Within this phase, which has a Ca-aluminosilicate (and K-rich) composition, very abundant pyroxene-type crystals with highly sharp edges crystallized, chiefly prism-shaped and hollow skeletal crystals of diopside (Fig. 3e and f). The larger crystals seem to have grown suddenly following self-organization and spiral growth with slight misorientation at the interface. The crystals share a common crystallographic orientation, in line with the "imperfect oriented attachment" described by Penn and Banfield (1998). As a result, larger crystals appear to have grown out of smaller crystallites, thus depleting the calcium and magnesium from the matrix. Fe-rich bright crystals were also detected and may correspond to a fassaite-type pyroxene (Fig. 4j), i.e., a calcium–magnesium silicate with abundant aluminum and ferric iron, which could also be referred to as a "ceramic pyroxene" (Dondi et al., 1998). This generic clinopyroxene is formed between 800 and 1000 °C, and its chemical composition shows analogies with the synthetic fassaitic clinopyroxene, formed by diopside ($CaMgSi_2O_6$), Ca tschermakite or kushiroite ($CaAl_2SiO_6$), and esseneite ($CaFe^{3+}AlSiO_6$) components (Sakata, 1957; Akasaka and Onuma, 1980). The detection of fassaite may suggest the presence of chloritic clays in that chlorite is a typical clay mineral occurring alongside illite in the clayey materials found in the Veneto Valley (Maritan, 2004). Chlorite may therefore enhance fassaite formation because iron and aluminum are released during its breakdown (Yardley, 1993). Fassaite could also be formed from an amorphous phase rich in iron and magnesium (Grapes, 2006).

Wollastonite crystals were occasionally formed around rounded quartz grains, which suggests that firing temperatures of over 950 °C must have been reached in some parts of the bodies. In many samples in which the pyroxene-type crystals nucleated from the Ca-aluminosilicate phase are abundant, large prism-shaped pores can be observed within the Si-rich amorphous phase formed from the reaction with the quartz grains (1 in Fig. 4a–c). As the shape of these pores resembles that of the diopside crystals, it is possible that pyroxene phases could have formed there during firing and then "dissolved". Given that silicates can dissolve in alkaline environments, this may have been caused by the action of Ca-rich solutions after the bricks had been laid in the walls. These polygonal pores observed in the Si-rich portion around the quartz grains could confirm this process. The dissolution process might be encouraged by the composition of the pyroxene-type crystals that might be hosted there and/or of the Si-rich amorphous phase. It might also be enhanced by the fact that the contact area with the quartz grains is closely related to the open porosity, in communication with the surrounding environment. As a result, the pyroxene-type crystals formed within the Si-rich portion dissolved, while those formed within the Ca-aluminosilicate phase were not affected.

3.3.1 Transformation of the Mg-rich clayey grains to Mg-silicate mineral phases

The Ca- and/or Mg-rich microcrystalline clayey grains/lumps are probably related to the reprecipitation of carbonates within the pristine clayey sediments (Cucato et al., 2008) that were differentially transformed during firing, mainly depending on the original magnesium and calcium contents, the particle size, and the firing temperatures reached.

Different transformations of the Mg clayey grains can be observed: (i) early melilite rims and rings of Mg-rich crystals at the grain edges, with the pristine microcrystalline texture being quite well preserved at lower temperatures (Fig. 4d); (ii) varying degrees of nucleation achieved by the Mg-silicate crystals as the firing temperature increased (Fig. 4e); and (iii) inclusions transformed into Mg-silicate mineral phases with fully developed melilite reaction rims (Fig. 4f) at the highest temperatures. The higher the firing temperatures, the more transformed the pristine grains are. The formation of Mg-silicate crystals represents the highest degree of transformation as firing temperatures increase. As stated by Pérez-Monserrat et al. (2021), this differential transformation could be used as marker of both the firing temperatures and the base clay composition and provenance.

The microchemical analysis of these crystals indicates that the early Mg-rich silicate crystals have a composition similar to that of a monticellite ($Ca(Mg,Fe)SiO_4$) (Ca-olivine phase) (Fig. 4d). Their composition progressively changes to that of a Mg-pyroxene-type enstatite ($MgSiO_3$) and/or a Mg-olivine-phase forsterite (Mg_2SiO_4) (Fig. 4e and f). As firing temperature increases, the Mg and Si content rise and they become better ordered. Although the structure of monticellite and enstatite may host iron, the Fe-rich crystals occasionally detected (Fig. 4g) suggest that Mg^{2+} has been replaced by Fe^{2+} within the structure of the forsterite crystals. The occurrence of elements that are not normally components of these phases and/or the higher mobility of ions at such high temperatures should also be considered (Cultrone and Carrillo, 2020). Secondary electron images enabled us to observe the change in the morphology of the Mg-rich crystals as temper-

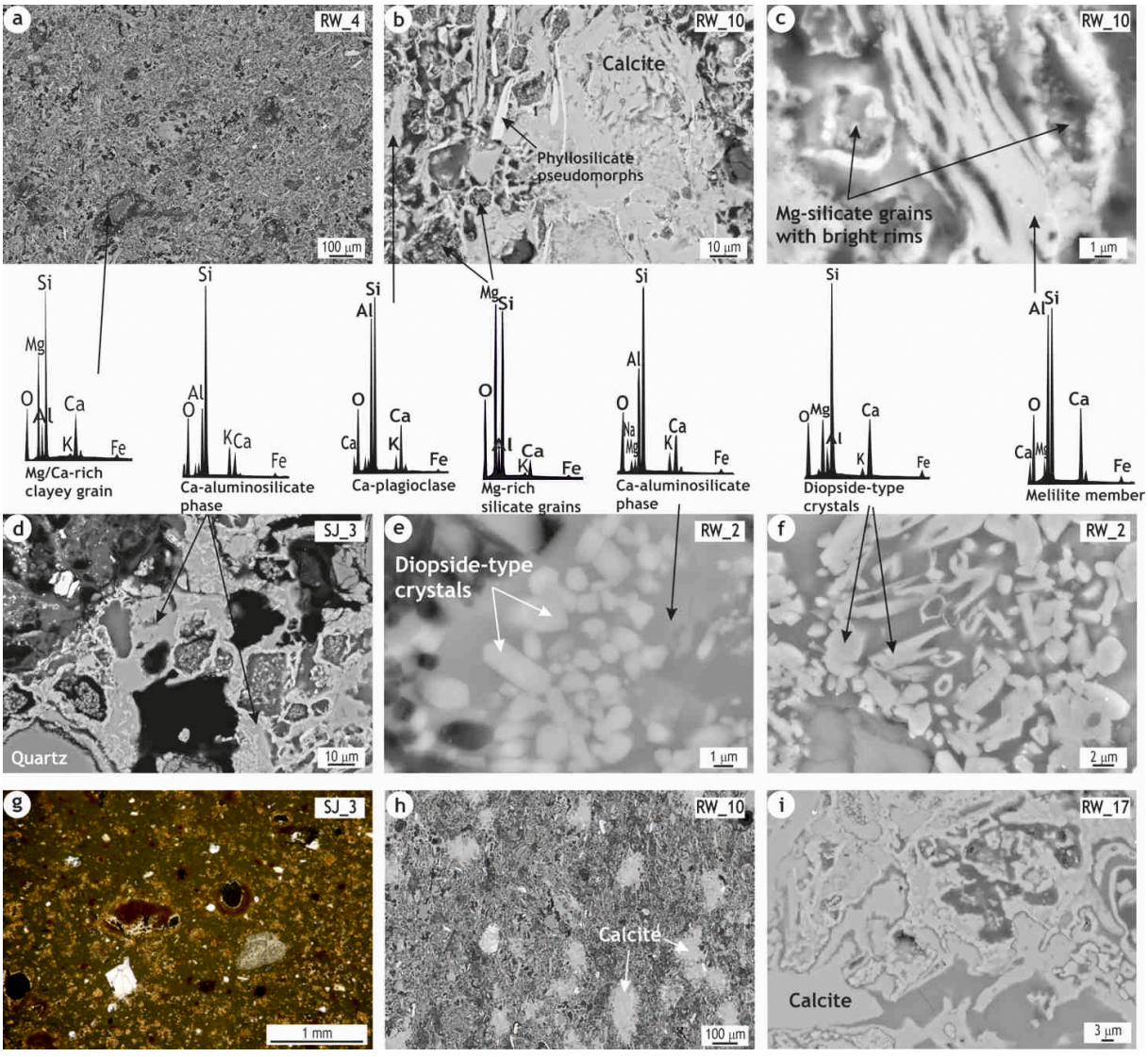

Figure 3. POM and HRSEM BSE images and associated EDS spectra showing some features of the $CHCB_2$ ceramic samples. **(a)** General view of the compact areas of the matrix where a coarse Mg-/Ca-rich clayey microcrystalline grain is observed; **(b)** oriented crystals of anorthite and phyllosilicate pseudomorphs and recarbonated calcite; **(c)** melilite member formed after the partial melting of phyllosilicate and Mg-rich silicate grains with bright reaction rims; **(d)** components of the brick sample bound by a Ca-aluminosilicate amorphous phase; **(e, f)** basal and longitudinal sections of prism-shaped and hollow skeletal crystals of diopside – with very sharp edges – nucleated from the amorphous phase, with a Ca-aluminosilicate composition; **(g)** sample observed by POM (cross-polarized light), in which the optically inactive portions correspond to the amorphous phase and the highly active areas mainly to clusters of recarbonated calcite crystals; **(h)** recarbonated calcite and **(i)** calcite precipitated, both through the groundmass.

ature increased, from plate- to glomerulus-shaped (Fig. 4h and i).

The Ca-rich clayey grains/lumps show a different decomposition path in which porous areas appear, mainly due to CO_2 release with increasing temperature (Fig. 4j). The original fine particles of calcite were completely consumed at high temperatures, thus leaving voids – *calcite ghosts* – occasionally with rhombohedral shapes (Fig. 4k).

3.3.2 Zeolite and calcite secondary-phase formation

Coarse and subrounded inclusions of calcite with a dark corona-like microstructure (developed during firing) were observed in many samples (Fig. 5a and b). These correspond to primary calcite from the base clays, as the local sands are rich in limestones (Jobstraibitzer and Malesani, 1973). These inclusions were largely preserved during firing, only reacting along the borders with the surrounding groundmass. Therefore, the initial decomposition of the calcite grains yielded

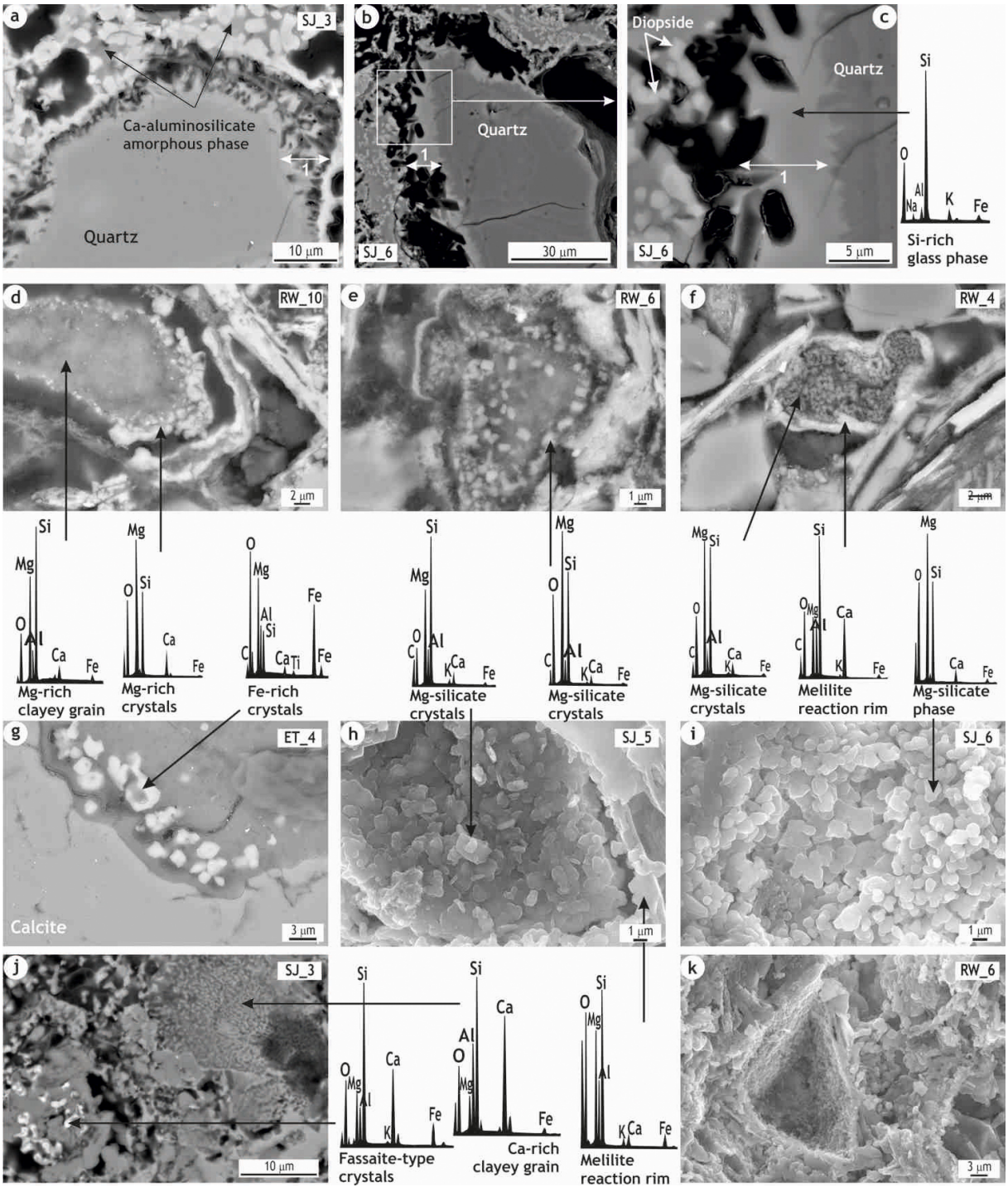

Figure 4. HRSEM BSE/SE images and associated EDS spectra of specific features observed in the ceramic bodies. **(a)** Pores within the silicate amorphous phase produced by quartz boundary transformation (1), next to the Ca-aluminosilicate phase where diopside crystals nucleated; **(b, c)** detail of the pores and quartz edge; these pores have the same shape as the pyroxene-type crystals they may once have hosted – note the large polygonal pores maybe due to the dissolution of the silicate phase (1) by Ca-rich solutions once the bricks were laid, as suggested; **(d)** early melilite rim and ring of Mg-rich crystals at the Mg clayey grain boundary; **(e)** differential nucleation of the Mg-silicate mineral phases; **(f)** heavily reacted Mg clayey grain, which was totally transformed into Mg-silicate crystals, and a well-developed melilite reaction rim; **(g)** Fe-rich crystals probably corresponding to an intermediate member of the forsterite–fayalite solid solution; **(h, i)** SE images of the Mg-silicate phases, with plate shapes evolving to rounded morphologies with the increase in temperature; **(j)** partially decomposed Ca-rich clayey particle and development of fassaite-type pyroxenes; **(k)** rhombohedral shape void formed due to the total consumption of a pristine carbonate grain.

dark rims at temperatures of 700–750 °C (Fabbri et al., 2014) and light melilite reaction rims at higher temperatures (800–850 °C). These were the first- and second-stage reaction domains, respectively (Tschegg et al., 2009).

Within the most altered areas of these coarse carbonatic grains, cubic and fan-shaped crystals of CaK zeolite were formed (Fig. 5c). Even though the presence of wairakite and/or chabazite-Ca as secondary hydration products has been previously suggested, the substantial potassium and calcium contents point more towards the formation of phillipsite-K ($(K,Na,Ca)_{1\text{-}2}(Si,Al)_8O_{16} \cdot 6H_2O$), enhanced by both the highly humid conditions and the circulation of alkaline solutions in the constructions where the bricks are laid. In fact, zeolites can be synthetized by alkali activation (Palomo et al., 2019) and fan-shaped phillipsite crystals with pozzolanic behavior and cementitious properties crystallized in situ at earth surface temperatures in alkaline aqueous environments as alkali-activated mineral cements in Roman marine concretes (Jackson et al., 2017).

Secondary calcite was significantly developed. Some recarbonated through the micromass, but most precipitated within the pores. The recarbonated calcite appears above all as clusters of sparitic and/or micro-sparitic crystals scattered through the groundmass (Fig. 3g and h) and is probably the result of carbonate and calcium transported by rainwater from the lime binder mortars commonly used in the city's historic buildings (Secco et al., 2018; Addis et al., 2019). The precipitated calcite partially fills the pores (Fig. 5g and h), the needle-shaped crystals indicating that they likely correspond to aragonite, and occasionally causes internal fractures in the carbonatic microcrystalline grains. The sealing of the shrinkage rims and the growth of calcite crystals on transformed carbonate grains (Fig. 5i and j) can also be observed. Another interesting finding was the precipitation in many samples of a calcite with a highly even texture (Fig. 3i). Besides being spread widely through the matrix, this smooth calcite completely sealed the shrinkage rims (Figs. 4g and 5k) and even filled the spaces left between the exfoliated basal planes of the phyllosilicates due to dihydroxylation. Abundant scalenohedral crystals were formed, mainly inside the pores (Fig. 5l and m). These morphologies, known as *dogtooth spar*, highlight the fast growth of the calcite crystals along the *c* axis and indicate an excess of Ca^{2+} ions, being the scalenohedral-to-rhombohedral transformation kinetically fostered with the increase in the carbonate content (Cizer et al., 2012).

It is possible that the precipitated calcite was formed both when the bricks were soaked in water and/or due to the circulation of Ca-rich solutions when the bricks were laid. During the firing, the CaO released by the decomposition of the carbonatic particles reacted with the silicate matrix to form the Ca-rich silicates. Although the free lime was almost eliminated due to the high temperatures reached, given the very high calcareous content of the pastes, it seems likely that the bricks were soaked in water just after firing. This practice considerably reduced the hydration of free lime (portlandite) and the further carbonation that takes place if bricks are exposed to the air after firing. In this way it helps prevent the formation of cracks due to the increase in volume caused by the formation of portlandite (Elert et al., 2003), defect known as "lime blowing". Soaking the bricks in water removes the CaO, which is very reactive and has poor consistency. The CaO precipitates as calcite on the surface of the water and/or within the pores of the bricks, thus minimizing the risk of lime blowing (Saenz et al., 2019). In addition, the uniformity of the even-textured calcite that was widely extended through some of the samples suggests that it formed quickly, at almost the same time as the soluble lime was removed (or redistributed within the pores of the brick, where it crystallizes as a secondary phase). Given that the waters that flow through the city of Padua (in rivers, canals, underground waters, etc.) are Ca-rich, it seems likely that the calcite also precipitates from aqueous solutions often in direct contact with the buildings of which the bricks form a part.

4 Discussion

The quite uniform chemical and mineralogical composition of the $CHCB_2$ samples points out that similar raw clays (very calcareous and particularly rich in Mg) and firing temperatures (from 900 to over 950 °C) were used in the brickmaking process. These yellow- and beige-colored bricks were sampled from diverse buildings from different periods in the city's construction history. This indicates that for many centuries bricks of this kind were produced using similar georesources (clayey material) and manufacturing technologies. However, the variability in the compositional range (Fig. 1 and Table 3), the different quantities of the mineral phases (Table 2), and the diverse intensity and irregular distribution of the microstructural transformations accomplished during firing (Figs. 3–5) indicate heterogeneities in the production processes. It is possible that the composition and texture of the raw clays varied to some extent, with silicate and calcite inclusions as well as Ca- and/or Mg-rich clayey grains that are heterogeneous in size and shape. Although the appearance of these carbonate clay lumps indicates that the raw clays were not sufficiently kneaded and/or left to rest before shaping (Maritan, 2004; Fabbri et al., 2014), it is also important to bear in mind that the silica, alumina, lime and/or periclase released via the decomposition of these lumps contributed significantly to the formation of the high-temperature phases. Other possible heterogeneities in the production processes could include the irregular distribution and dispersion of the heat inside the kiln and/or the varying duration of the firing process. As a result of these inconsistent firing procedures, it is possible that the bricks were fired at different temperatures according to their position inside the kilns and even that micro-domains appeared, with diverse transformation phases taking place within the same brick.

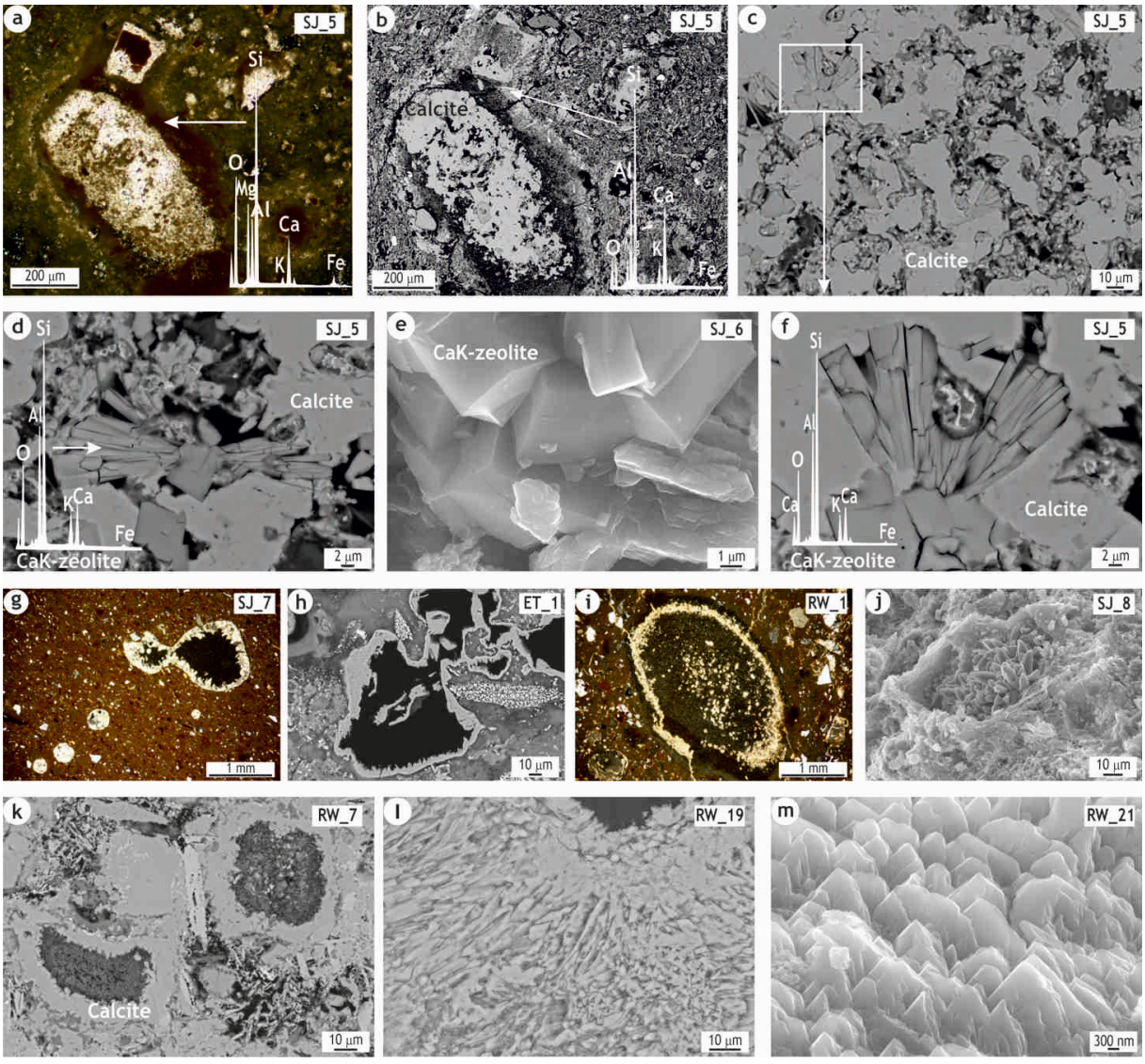

Figure 5. POM and HRSEM BSE/SE images and some EDS spectra on secondary zeolite and calcite. **(a, b)** Coarse calcite grain with dark corona-like microstructure observed by POM and HRSEM and EDS spectra of the first-stage (dark, **a**) and second-stage (light, **b**) reaction domains; **(c)** zeolite crystals formed within the more altered areas of the coarse calcite grains; **(d, e, f)** detailed images of the cubic and fan-shaped CaK-zeolite crystals, probably corresponding to phillipsite-K; **(g, h)** needle-shaped crystals of precipitated calcite partially filling the pores (sample belonging to $CHCB_1$); **(i, j)** precipitated calcite crystals filling shrinkage rims (sample belonging to $CHCB_1$) and/or grown over a slightly decomposed carbonate grain; **(k)** smooth precipitated calcite filling shrinkage rims; **(l, m)** scalenohedral crystals of calcite – *dogtooth growth* – preferably oriented in line with the *c* axis.

The profuse nucleation of the pyroxene-type crystals indicates that a firing technique involving rapid heating and/or soaking was used. It seems that the heating rate was faster than the nucleation and growth of the phases (Grapes, 2006) and/or that some reactions remained incomplete due to the bricks being removed from the kiln too early. It must have been a highly reactive, supersaturated system (Ca-rich and also rich in Mg and Al), which was enhanced in turn by the fine grain of carbonate inclusions, where small pyroxene-type crystals grew fast and early by direct nucleation from the melt (the Ca-aluminosilicate amorphous phase). Likewise, the reactivity of the system was increased by the fact that the crystals were very small, in turn giving rise to very intensive nucleation. Although within a meta-stable system like raw clays under firing, reactions can be delayed. However, in this highly reactive, supersaturated system, some reactions may have taken place earlier. The occurrence of prism-shaped crystals, which had enough time to grow properly, and skeletal-shaped crystals, which did not, indicates that heat inputs of irregular intensity might have taken place

inside the kiln. Uneven conditions like these were also reflected in the occurrence (and the quantity) of different mineral phases (Table 2). Therefore, low quantities of newly formed silicates may be due to a fast heating rate and/or excessively short heating time, whereas higher quantities indicate more accurate, better-quality firing, in which the reactions between lime and periclase and the silicate matrix were completed (Fabbri et al., 2014).

Despite this variability in the production process, it is clear that the bricks are in a good state of conservation, a situation that can largely be attributed to the base clays. The firing of the calcareous-rich clays caused the development of an extensive Ca-aluminosilicate amorphous phase during firing, which enhanced the binding action inside the bricks. In fact, the loss of this phase was observed in other similar bricks in the city, prompting the granular disaggregation of the bodies (Pérez-Monserrat et al., 2022). The presence of magnesium can increase the strength of ceramic products (Lagzdina et al., 1998), which is also improved by the copious nucleation of the diopside-type crystals.

The decarbonization of the calcareous-rich clays and the incipient vitrification achieved produced quite porous bricks. This highly porous texture made them ideal for use in areas with high levels of humidity (such as those in the city of Padua). It could also be beneficial for brick conservation as it facilitates the uptake and movement of water inside them. In addition, due to the surrounding humidity, it is possible that the moisture gradient between the surface of the bricks and the nearby environment was quite low, thus enabling the humidity conditions within the bricks to remain fairly constant. Furthermore, this high porosity yielded plenty of spaces that were suitable for precipitation, almost all of which were filled by secondary calcite, which significantly increased the cementation of the bricks. The Ca-rich waters of the city and the lime mortars used to bind the bricks together played an essential role in the precipitation of this secondary calcite.

5 Conclusions

This research centered around a multi-analytical study of fired bricks from four emblematic heritage constructions in the city of Padua (northeastern Italy). More than half the bricks studied are yellow or beige in color and are well preserved. These bricks, corresponding to $CHCB_2$ ceramic bodies, were made out of Mg-rich calcareous illitic clays and were fired at high temperatures (from 900 to over 950 °C), at which incipient vitrification was achieved. These findings are in concordance with the data provided by Pérez-Monserrat et al. (2021, 2022), who found that these are the most representative type of brick in Padua and have shaped much of the city's built heritage.

The results suggest that the $CHCB_2$ ceramic bodies were manufactured under non-standard, often irregular conditions. Two main processes occurred during firing: (i) the development of a Ca-aluminosilicate amorphous phase where very abundant pyroxene-type crystals nucleated and (ii) the transformation of the pristine Mg-rich clayey grains into Mg-silicate phases. While the high carbonate content obstructed the sintering process, the heterogeneous firing dynamics hindered more uniform transformations within the bricks. It is worth highlighting the formation of a phillipsite-K (zeolite) secondary phase within the coarse calcite grains, which was chiefly enhanced by the high calcium content of the bodies and the high levels of humidity in some areas of the constructions of which the bricks formed a part. Another interesting finding was the uniform secondary calcite that widely precipitated through the groundmass.

The information obtained in this multi-analytical study has increased the knowledge of (i) the mineralogical and microstructural transformations that take place when very calcareous – especially rich in magnesium – and highly unevenly textured clays are fired at over 900 °C and (ii) the formation of secondary phases within highly calcareous bricks laid in highly humid environments in an area with Ca-rich waters. These bricks are very representative of those used in Padua's historic monuments and have played a key role in shaping the city. Their high quality has also enhanced the preservation of this built heritage, due largely to the specific base raw clays that were used and the high firing temperatures that were reached, which yielded high-quality bricks in spite of an often irregular production process. The durability of the bricks was also enhanced post-firing by processes involving the high levels of humidity in the city and the calcareous waters that run through it.

Data availability. No data sets were used in this article.

Author contributions. EMPM, LM and GC conceptualized the research and methodology and interpreted the results. EMPM carried out the formal analysis, supervised the investigations and wrote the original draft; LM facilitated spectrophotometry, POM and XRPD resources and revised the original draft; GC enabled the use of HRSEM-EDS resources and revised the original draft.

Competing interests. The contact author has declared that neither they nor their co-authors have any competing interests.

Disclaimer. Publisher's note: Copernicus Publications remains neutral with regard to jurisdictional claims in published maps and institutional affiliations.

Special issue statement. This article is part of the special issue "Mineralogy of the built environment". It is not associated with a conference.

Acknowledgements. Special thanks are due to Edi Pezzetta and Monica Pregnolato from the Archeology, Fine Arts and Landscape Surveillance Department of Venice's metropolitan area and Belluno, Padua and Treviso provinces; Domenico Lo Bosco from the City Hall of Padua; and Valeria Zanini and Nicola Di Cicco from the National Institute of Astrophysics Astronomical Observatory of Padua for the sampling authorizations. The help and courtesy of Giulio Pagnoni, abbot of Saint Justine Benedictine Monastery; Marie-Ange Causarano from the Cultural Heritage Department of the University of Padua; Elisa Pagan from the City Hall of Padua; and Stefano Tuzzato during the sampling operations are gratefully acknowledged. The authors would also like to thank Francisco Coruña and Sol López de Andrés from the Research Assistance Center of the Faculty of Geological Science of the Complutense University of Madrid (Spain) for the XRF chemical analysis; Leonardo Tauro, Chiara Dalconi, Federico Zorzi and Marco Favero from the Department of Geosciences, University of Padua, for the assistance provided during the thin-section preparation and XRPD analysis; and Jesús Montes from the Faculty of Sciences of the University of Granada and José Damián Montes from the Scientific Instrumentation Centre of the University of Granada for their help preparing samples. The support provided by Alicia González, from the Centre for Scientific Instrumentation of the University of Granada, during the HRSEM-EDS analysis is also deeply appreciated. The authors would finally like to thank Luca Valentini, from the Department of Geosciences of the University of Padua, for the references provided in order to perform the thermodynamic calculations; Nigel Walkington for improving the English language; and the two anonymous reviewers for their thorough reviews and suggestions.

Financial support. This research has been supported by the Horizon 2020 Marie Skłodowska-Curie Individual Fellowship Action (grant no. 836122); the Consejería de Conocimiento, Investigación y Universidad, Junta de Andalucía, Spain (Research Group RNM-179); and the Ministerio de Economía y Competitividad, Spain (grant no. MAT2016-75889-R).

Review statement. This paper was edited by Gilberto Artioli and reviewed by two anonymous referees.

References

Addis, A., Secco, M., Marzaioli, F., Artioli, G., Arnau, A., Passariello, I., Terrasi, F., and Brogiolo, G.: Selecting the Most Reliable ^{14}C Dating Material Inside Mortars: The Origin of the Padua Cathedral, Radiocarbon, 61, 2, 375–393, https://doi.org/10.1017/RDC.2018.147, 2019.

Akasaka, M. and Onuma, K.: The join rich $CaMgSi_2O_6$–$CaFe^{3+}AlSiO_6$–$CaTiAl_2O_6$ and its bearing on the Ti-rich fassaitic pyroxenes, Contrib. Mineral. Petrol., 71, 301–312, 1980.

Alia, J. M., Edwards, H. G. M., Garcia-Navarro, F. J., Parras-Armenteros, J., and Sanchez-Jimenez, C. J.: Application of FT-Raman spectroscopy to quality control in brick clays firing process, Talanta, 50, 291–298, https://doi.org/10.1016/S0039-9140(99)00031-4, 1999.

Aras, A.: The change of phase composition in kaolinite- and illite-rich clay-based ceramic bodies, Appl. Clay Sci., 24, 257–269, https://doi.org/10.1016/j.clay.2003.08.012, 2004.

Buxeda i Garrigos, J. and Cau Ontiveros, M. A.: Identificación y significado de la calcita secundaria en cerámicas arqueológicas, Complutum, 6, 293–309, 1995.

Buxeda i Garrigos, J., Mommsen, H., and Tsolakidou, A.: Alterations of Na, K and Rb concentrations in Mycenean pottery and a proposed explanation using X-Ray Diffraction, Archaeometry, 44, 187–198, https://doi.org/10.1111/1475-4754.t01-1-00052, 2002.

Çelik, A., Kadir, S., Kapur, S., Zorlu, K., Akça, E., Akşit, Í., and Cebeci, Z.: The effect of high temperature minerals and microstructure on the compressive strength of bricks, Appl. Clay Sci., 169, 91–101, https://doi.org/10.1016/j.clay.2018.11.020, 2019.

Cizer, O., Rodriguez-Navarro, C., Ruiz-Agudo, E., Elsen J., Van Gemert, D., and Van Balen, K.: Phase and morphology evolution of calcium carbonate precipitated by carbonation of hydrated lime, J. Mater. Sci., 47, 6151–616, https://doi.org/10.1007/s10853-012-6535-7, 2012.

Cucato, M., de Vecchi, G. P., Mozzi, P., Abbà, T., Paiero, G., and Sedea, R. (Eds.): CARG Progetto, Note illustrative della Carta Geologica d'Italia alla scalla 1 : 50.000, Foglio 147, Padova Sud, Istituto Superiore per la Protezione e la Ricerca Ambientale (ISPRA), Regione del Veneto, Italia, https://www.isprambiente.gov.it/Media/carg/note_illustrative/147_Padova_Sud.pdf (last access: 19 December 2021), 2008.

Cultrone, G.: The use of Mount Etna volcanic ash in the production of bricks with good physical-mechanical performance: Converting a problematic waste product into a resource for the construction industry, Ceram. Int., 48, 5724–5736, https://doi.org/10.1016/j.ceramint.2021.11.119, 2022.

Cultrone, G. and Carrillo, F. J.: Growth of metastable phases during brick firing: Mineralogical and microtextural changes induced by the composition of the raw material and the presence of additives, Appl. Clay Sci., 185, 105419, https://doi.org/10.1016/j.clay.2019.105419, 2020.

Cultrone, G., Rodriguez-Navarro, C., Sebastian, E., Cazalla, O., and De la Torre, M. J.: Carbonate and silicate phase reactions during ceramic firing, Eur. J. Mineral., 13, 621–634, https://doi.org/10.1127/0935-1221/2001/0013-0621, 2001.

Cultrone, G., Molina, E., and Arizzi, A.: The combined use of petrographic, chemical and physical techniques to define the technological features of Iberian ceramics from the Canto Tortoso area (Granada, Spain), Ceram. Int., 40, 10803–10816, https://doi.org/10.1016/j.ceramint.2014.03.072, 2014.

Darweesh, H. H. M.: Building materials from siliceous clay and low grade dolomite rocks, Ceram. Int., 27, 45–50, https://doi.org/10.1016/S0272-8842(00)00040-7, 2001.

Duminuco, P., Messiga, B., and Riccardi, M. P.: Firing process of natural clays. Some microtextures and related phase compositions, Thermochim. Acta, 321, 185–190, https://doi.org/10.1016/S0040-6031(98)00458-4, 1998.

Daghmehchi, M., Omrani, H., Emami, M., and Nokandeh, J.: Mineralogical and thermo-chemical characteristics of the Hellenistic ceramics and raw clay from Qizlar Qal'eh (northeastern Iran), Mater. Charact., 120, 143–151, https://doi.org/10.1016/j.matchar.2016.08.030, 2016.

Dondi, M., Ercolani, G., Fabbri, B., and Marsigli, M.: An approach to the chemistry of pyroxenes formed during the firing of Ca-rich silicate ceramics, Clay Miner., 33, 443–452, https://doi.org/10.1180/000985598545741, 1998.

Donnici, S., Serandrei-Barbero, R., Bini, C., Bonardi, M., and Lezziero, A.: The Caranto Paleosol and its role in the early urbanization of Venice, Geoarchaeology, 26, 514–543, https://doi.org/10.1002/gea.20361, 2011.

Elert, K., Cultrone, G., Rodriguez-Navarro, C., and Sebastian, E.: Durability of bricks used in the conservation of historic buildings. Influence of composition and microstructure, J. Cult. Herit., 4, 91–99, https://doi.org/10.1016/S1296-2074(03)00020-7, 2003.

Elias, M. L. and Cultrone, G.: On the use of sodium chloride and calcined diatomite sludge as additives to improve the engineering properties of bricks made with a clay earth from Jun (Granada, Spain), Minerals, 9, 64, https://doi.org/10.3390/min9010064, 2019.

Everhart, J. O.: Use of auxiliary fluxes to improve structural clay bodies, Bull. Am. Ceram., 36, 268–271, 1957.

Fabbri, B., Gualtieri, S., and Shoval, S.: The presence of calcite in archaeological ceramics, J. Eur. Ceram. Soc., 34, 1899–1911, https://doi.org/10.1016/j.jeurceramsoc.2014.01.007, 2014.

García-Labiano, F., Abad, A., de Diego, L. F., Gayán, P., and Adánez, J.: Calcination of calcium-based sorbents at pressure in a broad range of CO_2 concentrations, Chem. Eng. Sci., 57, 2381–2393, https://doi.org/10.1016/S0009-2509(02)00137-9, 2002.

Germinario, L., Siegesmund, S., Maritan, L., Simon, K., and Mazzoli, C.: Trachyte weathering in the urban built environment related to air quality, Herit. Sci., 5, 44, https://doi.org/10.1186/s40494-017-0156-z, 2017.

Gliozzo, E.: Ceramic technology. How to reconstruct the firing process, Archaeol. Anthrop. Sci., 12, 260, https://doi.org/10.1007/s12520-020-01133-y, 2020.

Grapes, R. H.: Pyrometamorphism, Springer, Berlin, Germany, https://doi.org/10.1007/3-540-29454-6, 2006.

Heimann, R. B. and Maggetti, M.: Experiments on simulated burial of calcareous terra sigillata: mineralogical changes-preliminary results, in: Scientific studies in ancient ceramics, British Museum: Occasional Paper 19, edited by: Hughes, M. J., British Museum Press, London, United Kingdom, ID: 130165336, 163–177, 1981.

Heimann, R. B. and Maggetti, M.: The struggle between thermodynamics and kinetics: Phase evolution of ancient and historical ceramics, Eur. Mineral. Union Notes Mineral., 20, 233–281, https://doi.org/10.1180/EMU-notes.20.6, 2019.

Holland, T. J. B. and Powel, R.: An internally consistent thermodynamic data set for phases of petrological interest, J. Metamorph. Geol., 16, 309–343, 1998.

Iordanidis, A., Garcia-Guinea, J., and Karamitrou-Mentessidic, G.: Analytical study of ancient pottery from the archaeological site of Aiani, northern Greece, Mater. Charact., 60, 292–302, https://doi.org/10.1016/j.matchar.2008.08.0013, 2009.

Issi, A.: Estimation of ancient firing technique by the characterization of semi-fused, Hellenistic potsherds from Harabebezikan/Turkey, Ceram. Int., 38, 2375–2380, https://doi.org/10.1016/j.ceramint.2011.11.002, 2012.

Issi, A. and Kara, A.: An investigation of pottery production technology for the West Slope wares from Dorylaion (Eskişehir/Turkey), Bol. Soc. Esp. Ceram. V., 52, 42–47, https://doi.org/10.3989/cyv.52013, 2012.

Jackson, M. D., Mulcahy, S. R., Chen, H., Li, Y., Li, Q., Cappelletti, P., and Wenk, H. R.: Phillipsite and Al-tobermorite mineral cements produced through low-temperature water-rock reactions in Roman marine concrete, Am. Mineral., 102, 1435–1450, https://doi.org/10.2138/am-2017-5993CCBY, 2017.

Jobstraibitzer, P. and Malesani, P.: I sedimenti dei fiumi veneti, Mem. Soc. Geol. Ital., 12, 411–452, 1973.

Klaarenbeek, W.: The development of yellow calcareous bricks, Trans. Br. Ceram. Soc., 60, 738–772, 1961.

Khalfaoui, A. and Hajjaji, M.: A chloritic-illitic clay from Morocco: Temperature-time transformation and neoformation, Appl. Clay Sci., 45, 83–89, https://doi.org/10.1016/j.jeurceramsoc.2004.10.030, 2009.

Kingery, W. D. and Aronson, M.: The glazes of Luca Della Robbia, Faenza, 5, 221–224, 1990.

Kiseleva, I., Navrotski, A., Belitski, I., and Fursenko, B. A.: Thermochemistry of phase equilibria in calcium zeolites, Am. Mineral., 81, 658–667, 1996.

Lagzdina, S., Bidermanis, L., Liepins J., and Sedmalis, U.: Low temperature dolomitic ceramics, J. Eur. Ceram. Soc., 18, 1717–1720, https://doi.org/10.1016/S0955-2219(98)00100-9, 1998.

Madivate, C. M. de O., Malate, A. M., Verryn, S., and Loubser, M.: Energy requirement for firing porcelain, B. Chem. Soc. Ethiopa, 18, 1, 73–80, https://doi.org/10.4314/BCSE.V18I1.61640, 2004.

Maggetti, M., Neururer, C., and Ramseyer, D.: Temperature evolution inside a pot during experimental surface (bonfire) firing, Appl. Clay Sci., 53, 500–508, https://doi.org/10.1016/j.clay.2010.09.013, 2011.

Maritan, L.: Archaeometric study of Etruscan-Padan type pottery from the Veneto region: petrographic, mineralogical and geochemical-physical characterisation, Eur. J. Mineral., 16, 297–307, https://doi.org/10.1127/0935-1221/2004/0016-0297, 2004.

Maritan, L.: Ceramic abandonment: How to recognize post-depositional transformations, Archaeol. Anthropol. S., 12, 199, https://doi.org/10.1007/s12520-020-01141-y, 2020.

Maritan, L., Nodari, L., Mazzoli, C., Milano, A., and Russo, U.: Influence of firing conditions on ceramic products: Experimental study on clay rich in organic matter, Appl. Clay Sci., 31, 1–15, https://doi.org/10.1016/j.clay.2005.08.007, 2006.

Mozzi, P., Bini, C., Zilocchi, L., Becattini, R., and Mariotti Lippi, M.: Stratigraphy, palaeopedology and palynology of Late Pleistocene and Holocene deposits in the landward sector of the Lagoon of Venice (Italy), in relation to the Caranto Level, Il Quaternario, Italian Journal of Quaternary Sciences, 16, 193–210, 2003.

Nodari, L., Marcuz, E., Maritan, L., Mazzoli, C., and Russo, U.: Hematite nucleation and growth in the firing of carbonate-rich clay for pottery production, J. Eur. Ceram. Soc., 27, 4665–4673, https://doi.org/10.1016/j.jeurceramsoc.2007.03.031, 2007.

Pacheco-Torgal, F., Castro-Gomes, J., and Jalali, S.: Alkali-activated binders: A review-Part 1. Historical background, terminology, reaction mechanisms and hydration products, Constr. Build. Mater., 22, 1305–1314, https://doi.org/10.1016/j.conbuildmat.2007.10.015, 2008.

Palomo, A., Monteiro, P., Martauz, P., Bilek, V., and Fernández-Jiménez, A.: Hybrid binders: A journey from the past to a sustainable future (opus caementicium futurum), Cem. Concr. Res.,

124, 105829, https://doi.org/10.1016/j.cemconres.2019.105829, 2019.

Penn, R. L. and Banfield, J. F.: Imperfect oriented attachment: dislocation generation in defect-free nanocrystals, Science, 281, 969–971, 1998.

Pérez-Monserrat, E. M., Maritan, L., Garbin, E., and Cultrone, G.: Production technologies of ancient bricks from Padua, Italy: Changing colors and resistance over time, Minerals, 11, 744, https://doi.org/10.3390/min11070744, 2021.

Pérez-Monserrat, E. M., Causarano, M. A., Maritan, L., Chavarria, A., Brogiolo, G. P., and Cultrone, G.: Roman brick production technologies in Padua (Northern Italy) along the Late Antiquity and Medieval times: Durable bricks on high humid environs, J. Cult. Herit., 54, 12–20, https://doi.org/10.1016/j.culher.2022.01.007, 2022.

Peters, T. and Iberg, R.: Mineralogical changes during firing of calcium-rich bricks clays, Bull. Am. Ceram., 57, 503–509, 1978.

Rathossi, C. and Pontikes, Y.: Effect of firing temperature and atmosphere on ceramics made of NW Peloponnese clay sediments. Part I: Reaction paths, crystalline phases, microstructure and colour, J. Eur. Ceram. Soc., 30, 1841–1851, https://doi.org/10.1016/j.jeurceramsoc.2010.02.002, 2010.

Riccardi, M. P., Messiga, B., and Duminuco, P.: An approach to the dynamics of clay firing, Appl. Clay Sci., 15, 393–409, https://doi.org/10.1016/S0169-1317(99)00032-0, 1999.

Rodriguez-Navarro, C., Ruiz-Agudo, E., Luque, A., Rodriguez-Navarro, A.B., and Ortega-Huertas, M.: Thermal decomposition of calcite: Mechanisms of formation and textural evolution of CaO nanocrystals, Am. Mineral., 94, 578–593, https://doi.org/10.2138/am.2009.3021, 2009.

Rodriguez-Navarro, C., Kudlacz, K., and Ruiz-Agudo, E.: The mechanism of thermal decomposition of dolomite: New insights from 2D-XRD and TEM analyses, Am. Mineral., 97, 38–51, https://doi.org/10.2138/am.2011.3813, 2012.

Sakata, Y.: Unit-cell dimensions of synthetic aluminian diopsides, Jpn. J. Geol. Geogr., 28, 161–168, 1957.

Saenz, N., Sebastián, E., and Cultrone, G.: Analysis of tempered bricks: from raw materials and additives to fired bricks for use in construction and heritage conservation, Eur. J. Mineral., 31, 301–312, https://doi.org/10.1127/ejm/2019/0031-2832, 2019.

Schwedt, A., Mommsen, H., Zacharias, N., and Buxeda i Garrigos, J.: Analcime crystallization and compositional profiles-comparing approaches to detect post-depositional alterations in archaeological pottery, Archaeometry, 48, 237–251, https://doi.org/10.1111/j.1475-4754.2006.00254.x, 2006.

Secco, M., Addis, A., Artioli, G., Marzaioli, F., Passariello, I., and Terrasi, F.: I materiali leganti della Cappella degli Scrovegni e dell'Arena: analisi e datazioni, in: La Cappella degli Scrovegni nell'anfiteatro romano di Padova: nuove ricerche e questioni irrisolte, edited by: Deiana, R., Padova University Press, Padova, Italia, 101–116, 2018.

Shoval, S.: Mineralogical changes upon heating calcitic and dolomitic marl rocks, Thermochim. Acta, 135, 243–252, https://doi.org/10.1016/0040-6031(88)87393-3, 1988.

Shoval, S., Gaft, M., Beck, P., and Kirsh, Y.: The thermal behavior of limestone and monocrystalline calcite tempers during firing and their use in ancient vessels, J. Therm. Anal., 40, 263–273, 1993.

Sondi, I. and Juracic, M.: Whiting events and the formation of aragonite in the Mediterranean Karstic Marine Lakes: new evidence on its biologically induced organic origin, Sedimentology, 57, 85–95, https://doi.org/10.1111/j.1365-3091.2009.01090.x, 2010.

Sondi, I. and Slovenec, D.: The mineralogical characteristics of the Lamboglia 2 Roman-age amphorae from the Central Adriatic (Croatia), Archaeometry, 45, 251–262, https://doi.org/10.1111/1475-4754.00107, 2003.

Tenconi, M., Maritan, L., Leonardi, G., Prosdocimi, B., and Mazzoli, C.: Ceramic production and distribution in northeast Italy: study of a possible trade network between Friuli Venezia Giulia and Veneto regions during the final Bronze Age and early Iron Age through analysis of peculiar 'flared rim and flat lip' pottery, Appl. Clay. Sci., 82, 121–134, https://doi.org/10.1016/j.clay.2013.06.020, 2013.

Tite, M.: Technological investigations of Italian Renaissance ceramics, in: Italian renaissance pottery, edited by: Wilson, T., British Museum Press, London, United Kingdom, 280–285, 1991.

Toledo, D. R., dos Santos Jr., R. T., Faria, J. G., Carrio, L., Auler, T., and Vargas, H.: Gas release during clay firing and evolution of ceramic properties, App. Clay Sci., 27, 151–157, https://doi.org/10.1016/j.clay.2004.06.001, 2004.

Traoré, K., Kabre, T. S., and Blanchart, P.: Low temperature sintering of a clay for pottery from Burkina Faso, Appl. Clay Sci., 17, 279–292, https://doi.org/10.1016/S0169-1317(00)00020-X, 2000.

Trindade, M. J., Dias, M. I., Coroado, J., and Rocha, F.: Mineralogical transformations of calcareous rich clays with firing: a comparative study between calcite and dolomite rich clays from Algarve, Portugal, App. Clay Sci., 42, 345–355, https://doi.org/10.1016/j.clay.2008.02.008, 2009.

Tschegg, C., Ntaflos, T., and Hein, I.: Thermally triggered two-stage reaction of carbonates and clay during ceramic firing – A case study on Bronze Age Cypriot ceramics, App. Clay Sci., 43, 69–78, https://doi.org/10.1016/j.clay.2008.07.029, 2009.

UNE-EN 15886: Conservation of Cultural Property. Test Methods. Color Measurement of Surfaces, AENOR, Madrid, Spain, 2011.

Vedder, W. and Wilkins, R. W. T.: Dehydroxylation and rehydroxylation, oxidation and reduction of mica, Am. Miner., 54, 482–509, 1969.

Wang, G., Wang, H., and Zhang, N.: In situ high temperature X-ray diffraction study of illite, Appl. Clay Sci., 146, 254–263, https://doi.org/10.1016/j.clay.2017.06.006, 2017.

Warr, L. N.: IMA–CNMNC approved mineral symbols, Mineral. Mag., 85, 291–320, https://doi.org/10.1180/mgm.2021.43, 2021.

Webb, T. L.: Chemical aspects of the unsoundness and plasticity in building limes, South African Ind. Chemist., 6, 290–294, 1952.

Yardley, B.: Contact Metamorphism. Edited by: Kerrick, D.M., Washington D.C. (Mineralogical Society of America: Reviews in Mineralogy, Vol. 26), 1992, xvi 847 pp., Mineral. Mag., 57, 387, 359–360, https://doi.org/10.1180/minmag.1993.057.387.22, 1993.